HHS Public Access

Author manuscript

Nat Neurosci. Author manuscript; available in PMC 2016 May 18.

Published in final edited form as:

Nat Neurosci. 2015 December ; 18(12): 1746–1755. doi:10.1038/nn.4165.

G9a Is Essential for Epigenetic Silencing of K+ Channel Genes in Acute-to-Chronic Pain Transition

Geoffroy Laumet[1], **Judit Garriga**[2], **Shao-Rui Chen**[1], **Yuhao Zhang**[1], **De-Pei Li**[1], **Trevor M. Smith**[1], **Yingchun Dong**[1,3], **Jaroslav Jelinek**[2], **Matteo Cesaroni**[2], **Jean-Pierre Issa**[2], and **Hui-Lin Pan**[1]

[1]Center for Neuroscience and Pain Research, Department of Anesthesiology and Perioperative Medicine, The University of Texas MD Anderson Cancer Center, Houston, TX 77030, USA

[2]Fels Institute for Cancer Research and Molecular Biology, Temple University School of Medicine, Philadelphia, PA 19140, USA

[3]Department of Anesthesiology, Institute and Hospital of Stomatology, Nanjing University Medical School, Nanjing 210008, PR China

Abstract

Neuropathic pain is a debilitating clinical problem and difficult to treat. Nerve injury causes a long-lasting reduction in K^+ channel expression in the dorsal root ganglion (DRG), but little is known about the epigenetic mechanisms involved. Here we show that nerve injury increased H3K9me2 occupancy at *Kcna4, Kcnd2, Kcnq2* and *Kcnma1* promoters but did not affect DNA methylation levels of these genes in DRGs. Nerve injury increased activity of G9a, histone deacetylases and EZH2, but only G9a inhibition consistently restored K^+ channel expression. Selective G9a knockout in DRG neurons completely blocked K^+ channel silencing and chronic pain development after nerve injury. Remarkably, RNA sequencing analysis revealed that G9a inhibition not only reactivated 40 of 42 silenced K^+ channel genes but also normalized 638 genes down- or up-regulated by nerve injury. Thus G9a plays a dominant role in transcriptional repression of K^+ channels and in acute-to-chronic pain transition after nerve injury.

Correspondence should be addressed to Dr. Hui-Lin Pan, Department of Anesthesiology and Perioperative Medicine, Unit 110, The University of Texas MD Anderson Cancer Center, 1515 Holcombe Blvd., Houston, TX 77030. Tel: (713) 563-7467; Fax: (713) 794-4590; ; Email: huilinpan@mdanderson.org

Author contributions

G.L. performed biochemical and behavioral experiments and mouse breeding. S.-R.C. performed all surgeries, tissue extractions, and immunocytochemical experiments. Y.Z. performed ChIP-PCR experiments. J.G. and J.J. performed bisulfite sequencing experiments. J.G and M.C. performed RNA sequencing experiments. D.-P.L. and T.M.S. performed DRG neuron dissociation and electrophysiological recordings. Y.D. performed some immunocytochemical and behavioral experiments. G.L., J.G., S.-R.C., D.-P.L., T.M.S., J.J., M.C., J.-P.I. and H.-L.P. analyzed the data. H.-L.P. and J.-P.I. conceived the project and supervised the study. G.L. and H.-L.P. wrote the manuscript.

Competing financial interests

The authors declare no competing financial interests.

A **Supplementary Methods** checklist is available.

Introduction

Chronic neuropathic pain resulting from peripheral nerve injury can cause prolonged suffering and reduce the quality of life in patients. Current treatments for neuropathic pain symptoms are poorly effective owing to our limited knowledge of the molecular mechanisms underlying neuropathic pain development. Nerve injury causes abnormal hyperactivity of primary sensory nerves [1,2] and enduring changes in the expression of pro- and anti-nociceptive genes in the dorsal root ganglion (DRG) [3,4]. However, little is known about the mechanisms involved in the sustained alterations in gene transcription found in injured DRGs and their roles in neuropathic pain.

One of the hallmarks associated with neuropathic pain is the long-lasting down-regulation of many K^+ channel genes, including *Kcna4, Kcnd2, Kcnq2* and *Kcnma1,* in injured DRGs [5-8]. These K^+ channels are crucially involved in controlling the membrane potential and excitability of DRG neurons [9-11]. $K_V1.4$ (*Kcna4)* and $K_V4.2$ (*Kcnd2)* primarily constitute the transient "A-type" K^+ current [10,12], whereas $K_V7.2$ (*Kcnq2)*-mediated M-current critically regulates the resting membrane potential and neuronal excitability [9,13]. Large-conductance Ca^{2+}-activated K^+ (BK, *Kcnma1*) channels are involved in the feedback inhibition of the action potential frequency and Ca^{2+} influx [14,15]. Two predominant epigenetic mechanisms are DNA methylation and histone tail modifications, which are key regulators of long-lasting changes in the gene expression in post-mitotic neurons [16,17]. Histone modifications associated with transcriptionally inactive chromatin include histone deacetylation, histone H3 lysine 9 dimethylation (H3K9me2) and histone H3 lysine 27 trimethylation (H3K27me3), which are catalyzed by histone deacetylases (HDACs), the lysine dimethyltransferase G9a/G9a-like protein (GLP) and enhancer of zeste homolog-2 (EZH2), respectively [16,18,19]. It is not known whether DNA methylation and histone modifications play a role in the transcriptional silencing of K^+ channel genes in neuropathic pain.

Therefore, in the present study, we investigated the epigenetic mechanism involved in K^+ channel gene silencing in the DRG after nerve injury. We selected *Kcna4, Kcnd2, Kcnq2* and *Kcnma1* as representative K^+ channel genes in our study, because their expression levels influence the excitability of DRG neurons and pain sensitivity [6,7,11,12,20,21]. Our study provides novel evidence that nerve injury consistently increased the enrichment of H3K9me2 in the promoters of *Kcna4, Kcnd2, Kcnq2* and *Kcnma1.* G9a inhibition or knockout in the DRG restored K^+ channel expression and attenuated pain hypersensitivity. RNA sequencing analysis revealed that inhibiting G9a not only reactivated almost all silenced K^+ channel genes but also normalized the expression of many other genes altered by nerve injury. Thus, we uncovered a dominant role for G9a-mediated H3K9me2 methylation in the transcriptional silencing associated with neuroplasticity in neuropathic pain.

Results

Nerve injury diminishes K^+ channel expression in DRGs

The L5 and L6 spinal nerve ligation (SNL) is a well-characterized neuropathic pain model[22]. We first determined the time course of the expression levels of *Kcna4, Kcnd2, Kcnq2* and

Kcnma1 in the DRG after SNL in rats. SNL gradually reduced the mRNA levels of *Kcna4, Kcnd2, Kcnq2* and *Kcnma1* in the DRG over a 4-week period (Fig. 1a). The reduction in the mRNA levels of all four K^+ channels was profound and reached a maximum 3 weeks after SNL, suggesting that K^+ channel expression in the DRG is suppressed during the transition from acute to chronic pain after nerve injury. We also found that the UCSC Genome Browser does not annotate the correct transcriptional start sites (TSSs) for *Kcna4*. We identified a new upstream exon in the *Kcna4* gene in the rat DRG (Supplementary Fig. 1). SNL had no effect on the mRNA level of all four K^+ channels in dorsal spinal cords (Supplementary Fig. 2a).

Nerve injury upregulates HDACs, G9a, and EZH2 in DRGs

Increased activity of HDACs, G9a and EZH2 is associated with epigenetic gene silencing [18]. We therefore examined how nerve injury affects the expression levels of HDACs, G9a and EZH2. For HDACs, we selected two Class I HDACs (HDAC1 and HDAC2) and two Class II HDACs (HDAC4 and HDAC5), because these four HDACs are highly expressed in the nervous system [23]. Immunoblotting experiments indicated that SNL increased the protein levels of HDAC1, HDAC2, HDAC4, G9a and EZH2 in injured DRGs 3 weeks after surgery compared with sham controls (Fig. 1b,c). Also, SNL significantly increased the mRNA levels of *Hdac1, Hdac4, G9a* and *Ezh2* in the DRG (Supplementary Fig. 3a-f). SNL had no effect on the mRNA level of proliferation cell nuclear antigen, a cellular marker for proliferation, in the DRG (Supplementary Fig. 3g).

To determine whether increased HDACs, G9a and EZH2 expression levels are associated with an increase in their enzymatic activity, we measured the protein level of histone H3 acetylation, H3K9me2 and H3K27me3, which are the substrates of HDACs, G9a and EZH2, respectively. SNL decreased the H3 acetylation level and increased the H3K9me2 and H3K27me3 levels in the DRG (Fig. 1d,e). SNL had no significant effect on the protein levels of G9a and H3K9me2 in spinal cords (Supplementary Fig. 2b). These data indicate that nerve injury increases the expression and activity of HDACs, G9a and EZH2 in the DRG.

To determine the cellular distribution of HDACs, G9a, and EZH2 in the DRG, we performed double immunolabeling using a neuronal marker (NeuN) with HDAC1, HDAC2, HDAC4, HDAC5, G9a or EZH2. Confocal images show that the immunoreactivities of HDAC2, HDAC4, HDAC5, G9a and EZH2 were present predominantly in DRG neurons (Fig. 2a,b,d-f). However, HDAC1 was not expressed in DRG neurons (Fig. 2c), which is consistent with *in situ* hybridization data showing that HDAC1 is expressed principally in glial cells [23]. While G9a, HDAC2 and EZH2 were predominantly localized in the nucleus, HDAC4 and HDAC5 were present in both the nucleus and the cytoplasm in DRG neurons. SNL did not alter the cellular distribution of G9a, EZH2 or four HDACs in DRG neurons.

Nerve injury increases H3K9me2 occupancy at K^+ channel gene promoters

Because the global activity of HDACs, G9a and EZH2 was increased in the injured DRG, we next determined whether nerve injury affects histone modifications at the promoter regions of *Kcna4, Kcnd2, Kcnq2* and *Kcnma1*. We performed chromatin immunoprecipitation (ChIP) followed by quantitative PCR (ChIP-PCR). We selected two

activating histone marks (H3K4me3 and H3K9ac) and two repressive histone marks (H3K9me2 and H3K27me3) [18]. We first validated the ChIP antibodies and optimized ChIP-PCR procedures by using *Gapdh*, a highly expressed gene, and *Slc12a5*, a gene poorly expressed in the DRG [24], as the controls. H3K4me3 and H3K9ac were highly enriched at the *Gapdh* promoter but poorly enriched in the *Slc12a5* promoter. In contrast, the levels of H3K9me2 and H3K27me3 at the *Gapdh* promoter were very low, and their levels in the *Slc12a5* promoter were very high (Fig. 3a,b). These data suggest that these four histone marks are predictive for gene expression in the DRG.

SNL consistently increased the occupancy of H3K9me2 at the promoters of all four K^+ channel genes around their TSSs in the DRG (Fig. 3c-f). SNL significantly reduced the H3K9ac level at the *Kcna4* and *Kcnma1* promoters and the H3K4me3 level at the *Kcnd2* promoter region (Fig. 3c-f). However, SNL did not affect H3K27me3 enrichment in any of these gene promoters. Additional experiments showed consistent increases in H3K9me2 enrichment in two other promoter regions of all four K^+ channel genes in the injured DRG (Fig. 3g,h). Thus, nerve injury–induced down-regulation of *Kcna4, Kcnd2, Kcnq2* and *Kcnma1* in the DRG is associated with altered histone modifications, particularly a remarkable increase in the enrichment of G9a-dependent H3K9me2. These findings support the general concept that a closed chromatin structure contributes to nerve injury–induced transcriptional silencing of K^+ channel genes in the DRG.

Nerve injury has no effect on DNA methylation of K^+ channel gene promoters

DNA methylation is another important epigenetic mechanism regulating gene expression [16]. Therefore, we investigated whether nerve injury–induced down-regulation of *Kcna4, Kcnd2, Kcnq2* and *Kcnma1* are associated with changes in the DNA methylation patterns of these genes. Bisulfite sequencing data showed that the promoter regions of *Kcna4, Kcnd2, Kcnq2* and *Kcnma1* in the DRG had little methylation. SNL had no significant effect on the DNA methylation status at the promoter regions of any of these genes in the DRG (Fig. 3i-l). We confirmed these findings by measuring methylation content of these four genes using bisulfite pyrosequencing. In addition, using digital restriction enzyme analysis of methylation (DREAM), we analyzed DNA methylation levels of 80 CpG sites located within 1 kb from TSSs of 30 K^+ channel genes. None of the 80 CpG sites showed any significant changes in DNA methylation status in injured DRGs (Supplementary Table 1).

G9a plays a critical role in nerve injury-induced K^+ channel genes silencing

We next determined whether inhibition of the activity of G9a, EZH2 or HDACs could increase the expression levels of K^+ channels in the injured DRG. UNC0638 (10 μg), a highly selective G9a inhibitor [25], GSK503 (5 μg), a highly specific EZH2 inhibitor [26], and suberoylanilide hydroxamic acid (SAHA; 50 μg), a specific HDAC inhibitor [27], were used for this study. The doses of the inhibitors were selected on the basis of the dose-response effects in the *in vivo* behavioral experiments (Supplementary Fig. 4a-f) and the efficacy and specificity data (Supplementary Fig. 5a-f). Because intrathecal injections allow agents access directly to the DRG neurons [28,29], animals were treated daily via intrathecal injections for 8 days. As expected, intrathecal UNC0638 decreased the H3K9me2 protein level in the DRG. UNC0638 had no significant effects on the acetyl-H3 and H3K27me3

protein levels but significantly increased the H3K9ac protein level (Supplementary Fig. 5e,f). Notably, another G9a inhibitor, BIX-01294, also increases the H3K9ac protein level in the rat brain [30], which suggests a close association between G9a and HDACs at H3K9.

We determined how inhibition of G9a, EZH2 or HDACs affects the expression level of *Kcna4, Kcnd2, Kcnq2* and *Kcnma1* in the DRGs. UNC0638 consistently normalized the mRNA levels of all four K^+ channels in the injured DRG (Fig. 4a-d). Treatment with SAHA restored the mRNA levels of *Kcnd2, Kcnq2* and *Kcnma1* only. GSK503 largely normalized the mRNA levels of *Kcnd2, Kcnq2* and *Kcnma1* but decreased the *Kcna4* mRNA level in the injured DRG (Fig. 4a-d). We next sought to determine whether combined treatments of the above inhibitors could produce greater effects on K^+ channel gene expression than any one inhibitor alone. The three combination treatments caused much larger increases in the *Kcnq2* mRNA level in the injured DRG (Fig. 4c). These results underscore the concept that histone modifications do not occur in isolation; rather, their combinatorial effects mediate the transcriptional signature of genes within the DRG. Additionally, UNC0638 treatment rescued the protein levels of all the four K^+ channels in the DRG reduced by SNL (Fig. 4e,f).

Because our ChIP-PCR and pharmacological studies highlighted a dominant role of G9a in nerve injury–induced K^+ channel gene silencing, we used G9a-specific siRNA to validate the results obtained with UNC0638. We confirmed the efficacy and specificity of the G9a-siRNA in the DRG in rats (Fig. 4g,h). G9a-specific siRNA, but not control siRNA, normalized the mRNA levels of *Kcna4, Kcnd2, Kcnq2* and *Kcnma1* in the DRG of SNL rats (Fig. 4i). However, treatment with G9a-specific siRNA had no significant effect on the mRNA levels of the four K^+ channel genes in the DRG of sham rats (Fig. 4j). Together, these results indicate that increased G9a activity plays a critical role in the silencing of K^+ channel genes in the DRG by nerve injury.

G9a mediates nerve injury–induced reduction in Kv currents in DRG neurons

We next conducted electrophysiological experiments to determine whether G9a inhibition could restore Kv currents in DRG neurons reduced by nerve injury. We performed whole-cell Kv recordings in acutely dissociated DRG neurons from control rats and SNL rats treated intrathecally with UNC0638 (10 μg/day) or vehicle for 8 days. K^+ channels encoded by *Kcna4, Kcnd2, Kcnq2* and *Kcnma1* are distributed in different types of DRG neurons [5,7,10–12,21]. Because DRG neurons are highly heterogeneous, it was difficult to ensure that similar phenotypes of sensory neurons were sampled in the three groups. For this reason, we used isolectin B_4 (IB_4)–Alexa 594 dye, which can label a subgroup of live DRG neurons [10]. Double immunocytochemical analysis showed that SNL caused a 45% reduction in the number of IB_4-positive neurons but did not change appreciably the distribution of cell sizes of IB_4-labeled neurons in the DRG. UNC0638 treatment had no effect on the number and distribution of IB_4-positive DRG neurons in SNL rats (Supplementary Fig. 6). The peak amplitudes of total, transient A-type, and persistent non-A-type Kv currents of IB_4-positive neurons were significantly lower in SNL rats than in control rats (Fig. 5a-d). Treatment with UNC0638 largely restored the total, A-type and non-A-type Kv currents of IB_4-positive neurons in SNL rats (Fig. 5a-d). UNC0638 had no significant effect on voltage-dependent

activation of Kv currents in these neurons (Fig. 5e-g). These results highlight the functional significance of increased G9a activity in diminished K^+ channel expression/activity of DRG neurons in neuropathic pain.

G9a in DRG neurons is critically involved in neuropathic pain development

To directly determine whether increased activities of G9a, EZH2, and HDACs are involved in neuropathic pain, we measured the effects of intrathecal injection of UNC0638, GSK503 and SAHA on pain hypersensitivity in SNL rats. Intrathecal administration of UNC0638 for 8 days gradually restored the nociceptive threshold to the baseline level (Fig. 6a). UNC0638 also significantly attenuated tactile allodynia in SNL rats ($P < 0.001$; Fig. 6b). Treatment with SAHA or GSK503 for 8 days reduced hyperalgesia but had no effect on allodynia (Fig. 6a,b). SAHA, UNC0638 or GSK503 had no significant effect on the nociceptive and tactile thresholds in sham rats (Supplementary Fig. 4g,h).

We next determined whether any combination of the above inhibitors could produce a greater effect on pain hypersensitivity than any inhibitor alone. Of note, only UNC0638 plus SAHA fully restored the nociceptive and tactile thresholds of SNL rats to the baseline levels (Fig. 6c,d). Treatment with UNC0638 plus GSK503 produced an effect less than that of UNC0638 alone (Fig. 6c,d).

We used the siRNA approach to validate our findings with the G9a inhibitor. Intrathecal treatment with G9a-specific siRNA, but not control siRNA, significantly attenuated tactile allodynia ($P = 0.0081$, $F_{1, 22}=8.467$) and mechanical hyperalgesia ($P < 0.0001$, $F_{1,22}=31.82$) of SNL rats (Fig. 6e,f). G9a-specific siRNA had no significant effect on the nociceptive (154.2 ± 7.4 vs. 157.1 ± 4.7 g in control siRNA group, n = 12 rats) or tactile (22.50 ± 1.7 vs. 24.21 ± 1.1 g in control siRNA group, n = 12 rats) threshold of sham rats 3 weeks after surgery.

To validate the role of G9a in DRG neurons in diminished K^+ channel expression and pain hypersensitivity caused by nerve injury, we selectively deleted G9a in DRG neurons by crossing $G9a^{flox/flox}$ mice with the sensory neuron-specific Cre line $Advillin^{Cre/+}$ (ref. 31), which is referred to as G9a conditional KO mice. Conditional deletion of G9a was specific to the DRG and did not significantly alter baseline thermal and mechanical sensitivities (Fig. 7a,b). In control mice, spared nerve injury induced prolonged tactile allodynia and hyperalgesia (Fig. 7c,d) and reduced the mRNA level of *Kcna4, Kcnd2 and Kcnq2* in the DRG (Fig. 7e). Strikingly, in G9a conditional KO mice, spared nerve injury failed to cause persistent pain hypersensitivity and reduction in the expression level of these K^+ channels in the DRG (Fig. 7c,d,f). Collectively, our findings indicate that G9a in DRG neurons is critically involved in nerve injury-induced suppression of K^+ channel expression and in the transition from acute to chronic pain.

G9a inhibition normalizes genome-wide gene expression in the injured DRG

To determine whether increased G9a activity contributes to the genome-wide effects of nerve injury on gene expression, we used RNA sequencing to analyze the mRNA profile in the DRGs obtained from sham control and SNL rats treated with UNC0638 or vehicle. We mapped the sequences obtained from this experiment to 16,811 different rat genes. The

transcript values for UNC0638-treated SNL rats were closer to the values obtained from sham control rats (Supplementary Fig. 7a). From all the genes identified, 2,035 changed their expression values at least 2-fold in the injured DRGs when compared to the controls. Cluster analysis of expression values for this set of genes indicated that 832 were down-regulated and 1,205 were up-regulated. We performed ingenuity pathway analysis to identify canonical pathways in which these genes might play a role. Among the top ten, we identified pathways relevant to both neuronal regulation and inflammation (Supplementary Fig. 7b,c).

Because the four K^+ channel genes selected for our study were all silenced by nerve injury (Fig. 1a), we extended our analysis to all the 105 K^+ channels mapped in our sequencing experiments, independently of the fold change values. The heat map and dendrogram generated with the expression values for all the K^+ channels (including their auxiliary subunits) showed that the SNL samples clustered together and separated from the sham control. Moreover, UNC0638-treated SNL samples were closer to the sham control rats than the vehicle-treated SNL rats were (Fig. 8a, Supplementary Table 2). A total of 72 K^+ channel genes expressed at > 1 fragments per kilobase of transcript per million mapped reads, a threshold approximately equivalent to one copy per cell [32]. Remarkably, further analysis revealed that the expression of 42 K^+ channel genes was down-regulated by nerve injury and that 40 (95.2%) of them were restored close to the control levels by UNC0638 treatment (Fig. 8b). This result is in agreement with our ChIP-PCR data in which the repressive mark H3K9me2 was enriched at the promoter of four selected K^+ channel genes after nerve injury (Fig. 3c-h). When SNL rats were treated with UNC0638, G9a could not methylate H3K9; therefore the expression of suppressed genes was restored.

Because nerve injury-induced epigenetic silencing of K^+ channel expression in the DRG was largely due to increased G9a activity, we next asked what other genes behave similarly. We searched for genes whose expression levels changed at least two fold after nerve injury and for which, after UNC0638 treatment, the expression values were restored to levels comparable to the sham control. From the list of 2,035 genes that changed at least two fold in association with nerve injury, we identified 638 that had expression levels normalized to control values by UNC0638 (Fig. 8c, Supplementary Table 3). Strikingly, UNC0638 treatment not only restored those down-regulated by nerve injury (n = 396 genes) but also normalized those up-regulated by nerve injury (n = 242 genes) (Fig. 8c,d). Ingenuity Pathway Analysis of these 638 genes revealed enrichment of genes involved in pain-related regulatory pathways (Fig. 8e). These findings suggest that increased G9a activity is critically involved in altered expression of many genes associated with neuropathic pain and might be targeted for therapy.

Discussion

A major knowledge gap in neuropathic pain research is whether epigenetic changes serve to initiate and maintain nerve injury-induced abnormal gene expression in chronic pain. Many K^+ channels contribute to the regulation of the excitability of DRG neurons and pain hypersensitivity [10,12,21,33,34]. Knockdown of Kv1.2 or Kv9.1 in naïve animals induces pain hypersensitivity [34,35], and overexpression of Kv1.2 or Kir2.1 reduces neuropathic pain [36,37]. We found that nerve injury diminished K^+ channel expression within 3 weeks, a critical

period during which acute pain transitions to its chronic phase in this rat model. Of note, nerve injury also progressively reduces the expression levels of other voltage-gated K^+ channels, such as *Kcna2* [34], *Kcnd3* [38] and *Kcns1* [35] in the DRG. We focused on analyzing K^+ channel expression in the L5 and L6 injured DRG, because only minor gene expression changes occur in the intact neighboring L4 DRG in SNL rats [3]. Our data suggest that dynamic down-regulation of various types of K^+ channels in the DRG are involved in the initiation and maintenance of neuropathic pain through epigenetic reprogramming.

A salient finding of our study is that nerve injury consistently increased the repressive mark H3K9me2 occupancy at K^+ channel promoters in the DRG, which prompted our focus on G9a in this study. Although long non-coding RNA contributes to *Kcna2* silencing in injured DRGs [34], the roles of DNA methylation and histone modification in transcriptional silencing of K^+ channel expression in neuropathic pain had not been determined previously. H3K9 methylation is a highly conserved histone post-translational modification and is commonly linked to transcriptional repression. G9a and GLP are the primary enzymes for H3K9me2 [39,40] and exist predominantly as a G9a–GLP heteromeric complex that appears to be a functional H3K9 methyltransferase *in vivo* [41]. We found that nerve injury increased the global expression level and activity of G9a in the DRG. Furthermore, G9a inhibition restored the expression level of *Kcna4, Kcnd2, Kcnq2* and *Kcnma1* in injured DRGs, which is in agreement with the increased H3K9me2 enrichment at the promoter regions of these K^+ channel genes by nerve injury. In addition, we found that inhibiting G9a largely restored the Kv currents in DRG neurons diminished by nerve injury. These data provide functional evidence for the essential role of G9a-mediated histone modification in the transcriptional silencing of K^+ channel genes of DRG neurons in neuropathic pain.

We also provided novel evidence for the critical role of G9a in nerve injury–induced chronic pain. Recent studies on epigenetic control of pain have been largely limited to HDACs. HDAC inhibitors can reduce pain hypersensitivity caused by tissue inflammation and nerve injury [42,43]. In the present study, we determined the relative contribution of G9a, EZH2 and HDACs to pain hypersensitivity caused by nerve injury. Compared with the effects of EZH2 and HDAC inhibitors, inhibiting G9a most effectively reversed pain hypersensitivity in SNL rats. We also found that treatment with G9a-specific siRNA fully restored the expression of *Kcna4, Kcnd2, Kcnq2* and *Kcnma1* in injured DRGs and largely attenuated pain hypersensitivity. In addition, nerve injury failed to reduce the expression levels of these K^+ channels in mice lacking G9a in DRG neurons. Our findings support the idea that increased G9a activity plays a dominant role in neuropathic pain development. Nevertheless, it is difficult to determine to what extent the analgesic effect produced by G9a inhibition is attributable to its rescuing effect on K^+ channel expression. As shown by our RNA sequencing analysis, G9a inhibition restored the expression levels of many down-regulated and up-regulated genes that are involved in nociceptive signaling in the injured DRG; this restoration could also contribute to the analgesic effect of the G9a inhibitor. Regardless of the interpretations of the results, our study provides a new plausible mechanism underlying the analgesic effect of G9a inhibition on neuropathic pain. Because inhibition or knockdown of G9a had little effect on the K^+ channel gene expression or mechanical sensitivity in sham rats, the basal G9a activity in the normal DRG may be very low. It is not clear why G9a-specific siRNA knocked down the G9a level more effectively in injured DRGs than in

control DRGs. Nerve injury upregulates large-pore pannexin-1 channels in the DRG [44], which may increase the uptake of siRNA in injured DRGs. We found that inhibition or knockdown of G9a normalized hyperalgesia but only partially reduced tactile allodynia. Thus, G9a inhibition or knockdown may rescue the expression levels of K^+ channels more in high-threshold nociceptive neurons than in low-threshold sensory neurons. Remarkably, mice with genetic deletion of G9a in DRG neurons did not develop chronic pain, indicating that G9a in DRG neurons is the crucial epigenetic regulator involved in the transition from acute to chronic pain after nerve injury.

Because nerve injury-induced gene expression changes likely involve multiple epigenetic regulators, we explored potential interactions between G9a, HDACs and EZH2 in regulating K^+ channel expression and pain hypersensitivity. Notably, combined treatments with G9a and HDAC inhibitors produced significantly greater effects on K^+ channel expression levels and pain hypersensitivity than one inhibitor alone, suggesting a cooperative interaction between G9a and HDACs in the control of nerve injury-induced K^+ channel expression and neuropathic pain. This notion is supported by the findings that G9a inhibition not only reduced H3K9me2 levels but also increased H3K9ac levels [30]. The coordinated crosstalk between methylation and acetylation at H3K9 has been shown in other cells/tissues [45,46], which may explain why methylation inhibition can lead to increased acetylation at H3K9. On the other hand, the interaction between G9a and EZH2 seems to be complex. Combined treatments with G9a and EZH2 inhibitors produce a significantly smaller effect on pain hypersensitivity than the G9a inhibitor alone. Consistent with this finding, EZH2 inhibition further reduced the *kcna4* expression level in the injured DRG. Elucidating the integrated transcriptional network (i.e., co-repressors) involved in altered gene expression in neuropathic pain remains a challenging task.

Another major finding of our study is that G9a-mediated histone lysine methylation plays a vital role in genome-wide gene expression changes in the DRG caused by nerve injury. Nerve injury can cause up-regulation and down-regulation of thousands of genes, including those involved in axon regeneration, G protein signaling, immune responses, neurotrophins, and ion channels in the DRG, as shown in our study and previous reports [3,4]. Strikingly, our RNA sequencing data show that inhibiting G9a activity restored almost all the silenced K^+ channel genes in injured DRGs. Most important, G9a inhibition also normalized the expression levels of many other genes, both down-regulated and up-regulated, due to nerve injury. Many of these genes are related to serotonin receptors, calcium signaling, G-protein coupled receptors, axonal guidance, and other signaling pathways known to be important in neuropathic pain and nociceptive regulations. Because G9a is generally known for mediating the H3K9me2 mark associated with transcriptional repression, it was somewhat unexpected that G9a inhibition also normalized many up-regulated genes in injured DRG. Some studies suggest that G9a may also function as a co-activator [47–49]. The dual activities of G9a as a repressor and activator may depend on its interacting partners [47]. Another possibility is that enrichment of H3K9me2 and G9a at the gene coding regions promotes active gene expression, in contrast to their transcriptional repressive function when present at gene promoters [49]. In addition, G9a may repress a transcriptional repressor for those upregulated genes in injured DRGs. Our findings demonstrate that G9a plays a critical role in the

transcriptional repressing and activating of a large number of genes associated with epigenetic plasticity in neuropathic pain.

In summary, our study reveals a fascinating epigenetic mechanism for transcriptional gene silencing in neuropathic pain. Unlike previous studies focusing on one gene at a time, our study provides unique insight into the dominant role of G9a as a common shared mechanism for epigenetic silencing of almost all K^+ channels in the DRG in neuropathic pain. This new knowledge advances our understanding of epigenetic plasticity involved in neuropathic pain development. G9a may represent a promising epigenetic target for preventing and treating chronic neuropathic pain.

ONLINE METHODS

Animal model of neuropathic pain and intrathecal cannulation

A total of 410 male Sprague-Dawley rats (8-9 weeks old; Harlan Sprague-Dawley, Indianapolis, IN) were used for this study. All animals were housed (2-3 rats per cage) in a standard 12:12 light–dark cycle with normal illumination. Spinal nerve ligation (SNL) in rats was used in this study as the neuropathic pain model. Animals were anesthetized with 2-3% isoflurane, and the left L5 and L6 spinal nerves were isolated and ligated tightly with 4.0-silk suture under a surgical microscope, as described previously [22]. Age-matched sham control rats were used as the control group. The sample sizes were predetermined based on similar studies we published previously using the same approaches. The surgical preparation and experimental protocols were approved by the Animal Care and Use Committee at The University of Texas MD Anderson Cancer Center and conformed to the National Institutes of Health guidelines on the ethical care and use of animals.

To surgically implant an intrathecal catheter, rats were anesthetized with isoflurane, and a PE-10 tubing was inserted through an incision made in the cisternal membrane. The catheter was advanced ~8 cm caudal so that the tip of each catheter was positioned at the lumbar spinal level. Rats displaying signs of motor or neurological dysfunction were excluded and killed immediately with an overdose of phenobarbital (200 mg/kg, i.p.). The animals were allowed to recover for 4–5 days before intrathecal injections. Drugs were injected intrathecally in a 5-μl volume, which was followed by a 10-μl flush with normal saline. Suberoxylanilide hydroxamic acid (SAHA; Sigma-Aldrich, St Louis, MO) and UNC0638 (Sigma-Aldrich) were dissolved in dimethyl sulfoxide. GSK503 (GlaxoSmithKline Laboratories, Collegeville, PA) was dissolved in Captisol (Ligand Pharmaceuticals Inc., La Jolla, CA). The doses of these agents were selected on the basis of preliminary data and their effects on the activity of HDACs, G9a and EZH2. Drug treatment started 3 weeks after SNL when the chronic pain is well established.

A total of 46 mice were used in this study (8-10 weeks of age, both males and females, with sex and age matched). Wild-type mice with C57/BL6J genetic background were obtained from Jackson Laboratory (Bar Harbor, ME). We selectively deleted G9a in DRG neurons by crossing $G9a^{flox/flox}$ mice with the sensory neuron-specific Cre line $Advillin^{Cre/+}$ (ref. 31), which is referred to as G9a conditional KO mice. Male $Advillin^{Cre/+}$ mice (from Duke University) were used to cross to female $G9a^{flox/flox}$ mice first to obtain male $Advillin^{Cre/+}$:

G9a$^{flox/+}$ mice, which were crossed again to female G9a$^{flox/flox}$ mice to generate Advillin$^{Cre/+}$: G9a$^{flox/flox}$ (G9a conditional KO, maintained on C57/BL6J genetic background) mice. Neuropathic pain was induced using the mouse spared nerve injury model (SNI) [50]. Briefly, mice were anesthetized with isoflurane, and an incision was made on the left lateral thigh to expose the sciatic nerve. We ligated and sectioned the common peroneal and tibial nerves (leaving the sural nerve intact) under a surgical microscope. The sham procedure consisted of the same surgery without nerve ligation and section.

Behavioral assessment of nociception in rodents

To quantify tactile allodynia, rodents were placed in individual plastic boxes on a mesh floor and allowed to acclimate for 30–45 min. A series of calibrated von Frey filaments was applied perpendicularly to the plantar surface of the hindpaw with sufficient force to bend the filaments for 6 s, and brisk paw withdrawals or flinching was considered as a positive response. In the absence of a response, the filament of next greater force was applied. If a response occurred, the filament of next lower force was applied. The tactile stimulus producing a 50% likelihood of withdrawal was determined using the “up-down” calculating method [51].

We measured mechanical hyperalgesia in nerve-injured animals by testing the withdrawal threshold in response to a noxious pressure stimulus (Randall-Selitto test) using the paw pressure Analgesy-Meter (UgoBasile Biological Research, Comerio, Italy). When the animal displayed pain by either withdrawing the paw or vocalizing, the pedal was immediately released, and the nociceptive withdrawal threshold was read on the scale [6]. The investigator (G.L.) performing behavioral experiments was blinded to the treatments and the genotypes. All behavioral experiments were conducted between 10 am and 5 pm.

We quantified the heat and cold sensitivity in mice, as previously described [52]. The mice were placed in a Plexiglas cylinder on the metal plate and allowed to acclimate for 30 min. Using an incremental thermal plate (starting temperature 30 °C, ramp set at the maximum rate of 10 °C/min; PE34, IITC Life Science, Woodland Hills, CA), we recorded the temperature of the plate at the time when the hindpaw withdrawal response occurred.

Quantitative PCR

Animals were deeply anesthetized with sodium pentobarbital (60 mg/kg, i.p.), and the DRG and dorsal spinal cord tissues were rapidly removed (at L5 and L6 levels for rats, and at L3 and L4 levels for mice). Total RNA was extracted from the DRGs using the Trizol/chloroform total RNA extraction system and treated with DNase I (Invitrogen, Carlsbad, CA). cDNA was prepared by using the Superscript III first-strand synthesis kit and treated by RNase H (Invitrogen, Carlsbad, CA). Quantitative PCR was performed using the iQ5 real-time PCR detection system with the SYBR green PCR mix (Bioline, Taunton, MA). All samples were analyzed in triplicate using an annealing temperature of 60 °C. The primer pairs used for *Gapdh*, *Kcna4, Kcnd2, Kcnq2,* and *Kcnma1*, and histone-modifying enzymes are listed in Supplementary Table 4. Using a ten-fold dilution of the cDNA from the DRGs as the template, standard curves were generated to calculate the relative mRNA levels of different genes in the control and treatment groups. The relative amount of target genes in

each sample was first normalized to the level of a housekeeping gene, *Gapdh* [53], and then normalized to its expression level in sham rats. The PCR product specificity was verified by melting-curve analysis and agarose gel electrophoresis.

Western immunoblotting

DRG and dorsal spinal cord tissues at the L5 and L6 levels were removed, dissected, and homogenized in 300 μl RIPA buffer containing 50 mM Tris-HCl (pH 7.4), 1% NP-40, 0.25% Na-deoxycholate, 150 mM NaCl, 1 mM EDTA, 1 mM Na_3VO_4, and 1 mM NaF in the presence of proteinase inhibitor cocktail and an HDAC inhibitor, sodium butyrate (5 mM; Sigma-Aldrich). Samples were then put on ice for 30 min with shaking. Lysates were centrifuged at 13,000 g for 30 min at 4 °C. The supernatant was carefully collected, and the protein concentration was measured using a DC protein assay kit (Bio-Rad, Hercules, CA). Thirty μg of total proteins of each sample was loaded and separated on 4–12% Bis-Tris SDS-PAGE (Invitrogen, Carlsbad, CA). The resolved proteins were transferred to nitrocellulose membranes. The membranes were treated with 5% bovine serum albumin in Tris buffer containing Tween 20 (TNT) for 2 h and then incubated with one of the following primary antibodies overnight at 4°C: Kv1.4 (catalog #05-409, Upstate Biotechnology), Kv4.2 (catalog #APC-023, Alomone Labs), Kv7.2 (catalog #APC-050, Alomone Labs), BKα1 (catalog #APC-021, Alomone Labs), acetyl-H3 (catalog #06-599, Millipore), H3K9ac (catalog #39917, Active Motif), H3K27me3 (catalog #9733, Cell Signaling Technology), histone H3 (catalog #9715, Cell Signaling Technology), H3K9me2 (catalog #ab1220, Abcam), G9a (catalog #09-071, Millipore), HDAC1 (catalog #IMG-337, Imgenex), and HDAC2, HDAC4, HDAC5 and EZH2 (catalog #2540, #2072, #2082 and #5246, respectively; Cell Signaling Technology). The membrane was washed three times and then incubated with horseradish peroxidase–conjugated goat anti-rabbit secondary antibody (Jackson ImmunoResearch, West Grove, PA) for 1 h at room temperature. The protein band was revealed with an ECL Plus detection kit (ThermoFisher, Rockfort, IL), and the protein band intensity was quantified by using the ImageJ software program. The amounts of proteins were normalized by GAPDH (catalog #5174; Cell Signaling Technology), which was used as a protein loading control.

Double immunofluorescence labeling

To determine the effect of nerve injury on the cellular distribution HDAC1, HDAC2, HDAC4, HDAC5, G9a and EZH2, we performed double immunolabeling with a neuronal marker. NeuN (catalog #MAb377, Millipore) and one of the following epigenetic histone-modifying enzymes in the DRGs obtained from five rats 3 weeks after surgery: HDAC1 (catalog #19845, Abcam), HDAC2, HDAC4, HDAC5 and EZH2 (catalog #2540, #2072, #2082 and #5246, respectively; Cell Signaling), and G9a (#09-071, Millipore). Under deep anesthesia with sodium pentobarbital (60 mg/kg, i.p.), rats were perfused intracardially with 4% paraformaldehyde in 0.1 M phosphate-buffered saline (PBS) and 10% sucrose in PBS, pH 7.4. The L5/L6 DRGs were removed, frozen, post-fixed in the fixative solution for 2 h, and cryoprotected in 30% sucrose in PBS for 48 h at 4°C. The tissues were cut to 30 μm in thickness, collected free-floating in 0.1 M Tris-NaCl-Tween (TNT) buffer, rinsed in 0.1 M TBS, and blocked in 4% normal goat serum in TBS for 1 h [54]. The sections were then incubated with the mixture of primary antibodies diluted in TBS solution containing 2%

normal goat serum and 0.3% Triton X-100 for 2 h at room temperature and overnight at 4°C. Subsequently, sections were rinsed in TNT buffer and incubated with the secondary antibody mixture (Alexa Fluor-488 conjugated to goat anti-rabbit IgG, and Alexa Fluor-594 conjugated to goat anti-guinea pig IgG; dilution: 5 μg/ml) for 1.5 h. The sections were washed in TNT buffer three times and then rinsed in PBS for 30 min, mounted on slides, dried, and coverslipped. The sections were examined on a laser scanning confocal microscope (Zeiss, Germany). The antibodies used for immunocytochemistry were selected from previous publications: anti-G9a [55], anti-HDAC1 [56], anti-HDAC2 [57], anti-HDAC4 [57], anti-HDAC5 [57] and anti-EZH2 [58]. These antibodies showed a single protein band with the correct expected size in immunoblotting analysis, and omission of the primary antibodies resulted in negative labeling in all the DRG sections examined. In additional experiments, double labeling of IB_4-Alexa 594 (1:100; Invitrogen) and NeuN was used for characterization of the distribution of IB_4-positive DRG neurons from sham and SNL rats.

Bisulfite sequencing and pyrosequencing

To investigate the methylation pattern of CpG sites near the transcriptional start site (TSS) of four K^+ channel genes, methylation data obtained from the L5 and L6 DRGs of control and SNL rats 3 weeks after surgery were compared. Genomic DNA obtained from pools of DRGs was treated with bisulfite using an Epitek bisulfite kit (Qiagen). This process converts the unmethylated cytosine to uracil but leaves the methylated cytosine unchanged. Using specific primers, the regions of interest close to the TSS of *Kcna4*, *Kcnd2*, *Kcnq2*, and *Kcnma1* were amplified by PCR. The amplified DNA was cloned into 4-TOPO vector (Invitrogen), and the DNA obtained from individual clones after bacteria transformation was sequenced (Beckman Coulter Genomics). Each sequence, corresponding to a different allele, was analyzed for the presence of methylated cytosines using the QUMA web-based program (http://quma.cdb.riken.jp/). Primer sequences for bisulfate sequence are listed in Supplementary Table 4. Bisulfite-treated DNA obtained from the same samples was also analyzed by pyrosequencing technology using the PyroMarkQ24 platform (Qiagen).

Digital restriction enzyme analysis of methylation (DREAM)

DREAM analysis of K^+ channel genes was performed as we described previously [59]. In brief, genomic DNA extracted from DRG samples was spiked with methylation standards and sequentially digested with two restriction endonucleases recognizing CCCGGG sites in DNA. *SmaI* cut only unmethylated sites, and leaves blunt ends after cutting. Next, *XmaI* cleaved the remaining methylated sites and leaves a 5′ overhang sequence. Thus, specific signatures were created for methylated and unmethylated sites. Enzyme-treated DNA was then used to generate sequencing libraries according to Illumina protocols and run on an Illumina HiSeq 2000 and 2500. Sequencing data were mapped to the rat genome (rn4) and the reads with unmethylated and methylated signatures were counted at individual CCCGGG sites. Methylation level was calculated as the ratio of reads with the methylated signature to all reads mapping to the site.

ChIP-PCR

We performed chromatin immunoprecipitation (ChIP) using the Magna ChIP G tissue kit (Millipore; catalog #17-20000), according to the manufacturer's instructions. Briefly, fresh

DRG tissues were rapidly removed from anesthetized rats and were stabilized for 3 min using stabilization buffer. Then, the DRGs were incubated in 2% formaldehyde for 20 min at ~26 °C. After being washed three times with PBS, the DRGs were incubated in lysis buffer for 15 min on ice. Finally, the DRG tissues were sonicated (30 s on and 30 s off, repeated 200 times) in ChIP dilution buffer using a water bath sonicator (Qsonica, Newtown, CT) at 4 °C. The sonicated DRG samples were centrifuged at 12,000 rpm for 10 min at 4 °C. Chromatin was pulled down using the following antibodies: IgG (as a negative control; catalog #ab124055, Abcam), total H3 (catalog #2650s, Cell Signaling Technology), H3K9me2 (catalog #ab1220, Abcam), H3K9ac (catalog #39917, Active Motif), H3K27me3 (catalog #9773s, Cell Signaling Technology), and H3K4me3 (catalog #9751s, Cell Signaling Technology). After chromatin precipitation, we performed quantitative PCR using the primers described in Supplementary Table 4. Data were analyzed and corrected by input and total H3 conditions [60].

RNA sequencing

DRG samples were obtained from four vehicle-treated SNL, three UNC0638-treated SNL, and four sham control rats. We generated strand-specific RNA libraries from 1 μg of purified RNA using TruSeq stranded total RNA plus Ribo-zero kits (Illumina). Indexed libraries were normalized and pooled before sequencing. The sequencing was performed at the institutional genome sequencing facility. Single end reads (50 bp, average 20 million reads) per sample were obtained using the HiSeq 2500 platform from Illumina. The sequencing reads were aligned to the rat genome rn4 using TopHat [61], which takes into account reads coming from splicing junctions (parameters were set to default). The expression level of all RefSeq transcripts was evaluated using Cufflinks [62], and a FPKM (fragments per kilobase of transcript per million fragments mapped) was calculated for each transcript (the parameters were set to default and the rn4 RefSeq GTF table was used to define the transcripts). We utilized principal component analysis (PCA) to test the correlation among the normalized sequencing data. Differences in gene expression levels between samples were assessed with the Cuffdiff algorithm and calculated as log 2 (fold change). All the original RNA sequence data were deposited in the database repository of Gene Expression Omnibus (GEO accession #GSE59043).

siRNA knockdown of G9a

Three siRNA sequences targeting G9a and the universal negative control siRNA were purchased from Sigma-Aldrich (St. Louis, MO). We first validated and screened for the most effective G9a siRNA using the F11 DRG cell line, which was cultured in Dulbecco medium and 10% fetal bovine serum (Invitrogen, Carlsbad, CA). Cells were plated at 55% confluency on the day of the transfection. The transfection reagent iFect (Neuromics, Edina, MN) was mixed with 2 μg of siRNA and incubate for 24 h at 37 °C. Forty-eight h after transfection, the cells were harvested, and the RNA was isolated. For determination of G9a knockdown efficiency, quantitative PCR was performed to measure the G9a mRNA levels using the F11 cell samples treated with the control siRNA and siRNAs targeting G9a. The siRNA sequence (AGUAACGGGCAUCAAUGC) that was the most effective in knocking down G9a was selected and used for the *in vivo* study.

On the day of injection, siRNA was mixed with iFect to a final concentration 400 mg/l according to the protocol for intrathecal injection [29]. The G9a-specific siRNA (4 μg) and the control siRNA were administered intrathecally for 4 consecutive days in SNL rats. The DRG neuronal uptake of siRNA delivered using iFect upon intrathecal injections has been shown previously [29]. Twenty-four h after the last injection, the L5 and L6 DRGs were removed and used for PCR and Western blot analyses.

DRG neuron dissociation and recording of K^+ channel currents

Rats were deeply anesthetized with 2-3% isoflurane, and the L5/L6 DRGs were removed and immersed immediately into 1.5 ml sterile Eppendorf tubes with 1 ml of Hank's balanced salt solution (HBSS; pH 7.3–7.4). The attached nerve roots were trimmed, and the DRG neuronal dissociation was performed as previously described [63]. Briefly, the DRG tissue was incubated in 1 ml of HBSS containing papain (75 units/ml, Worthington Biochemical Co., Lakewood, NJ) at 37 °C for 20 min. Then, the solution containing DRG tissues was centrifuged, and the solution was replaced with 1 ml of HBSS containing type II collagenase (2,000 units/ml; Worthington Biochemical Co.) and type II dispase (5 units/ml; Roche Diagnostics, Indianapolis, IN) for another 20 min. After stopping the enzymatic digestion, complete F12 medium was used to re-suspend the DRG neurons. A glass pipette was used for gentle trituration to separate the neurons, which were applied directly onto coverslips that had been incubated with Poly-L-Ornithine. The neurons were then kept in an incubator at 37°C with 5% CO_2 for 2 h. The final recordings were performed 2–8 h after DRG dissociation.

The Kv currents of dissociated DRG neurons were recorded as we described previously [5,10]. The extracellular solution consisted of (in mM) 150 choline chloride, 5 KCl, 2 $CaCl_2$, 1 $MgCl_2$, 10 HEPES, 1 $CdCl_2$, and 10 D-glucose (pH 7.4 adjusted with KOH, 320 mOsm). The glass recording pipettes were filled with an internal solution consisting of (in mM) 120 potassium gluconate, 20 KCl, 2 $MgCl_2$, 10 EGTA, 10 HEPES, 5 Na_2-ATP, and 1 $CaCl_2$ (pH 7.2 adjusted with KOH, 300 mOsm). Live DRG neurons were labeled in IB_4-Alexa 594 (1:100; Invitrogen) solution for 1 min followed by a 2-min wash. IB_4-positive neurons were visualized using epifluorescence and differential interference contrast optics on an inverted microscope (IX70, Olympus, Tokyo, Japan). The whole-cell recording (holding potential, −80 mV) was performed using EPC-10 amplifier and Pulse software (HEKA Instruments, Lambrect, Germany). The total whole-cell Kv current was recorded using a series of depolarizing voltages from −70 to 60 mV (400-ms pulse duration) in 10-mV increments at 2-s intervals [10]. In some neurons, the transient A-type Kv currents were isolated by using an A-type Kv channel blocker, 3,4-diaminopyridine (DAP) [5]. DAP-sensitive A-type Kv currents were derived by subtracting the Kv currents recorded in the presence of 5 mM DAP (i.e., DAP-insensitive persistent/non-A-type currents) from the baseline total Kv currents. Signals were filtered at 1 kHz and digitized at 10 kHz. The investigator (D.-P.L.) was blinded to the treatment groups during the recording experiments.

Data analysis and statistics

All values are presented as means ± S.E.M. The electrophysiological data were analyzed using the PulseFit software program (HEKA Instruments). The whole-cell current–voltage

(I–V) curves for individual neurons were generated by calculating the peak outward current at each potential and normalizing to the cell capacitance. The conductance–voltage (G–V) curves were obtained with the Boltzmann equation: $G/G_{max} = 1/[1 + \exp(V_{0.5} - V_m/k)]$, where $V_{0.5}$ is the membrane potential at which 50% activation is observed, k is the slope of the function, and V_m is the membrane potential. To determine whether the treatment effects on mRNA and protein levels were statistically significant, we used the Mann–Whitney U test to compare two groups and one-way ANOVA followed by Dunnett's or Tukey's *post hoc* test to compare more than two groups. Two-way ANOVA followed by Bonferroni's *post hoc* test was used to determine significant differences between treatment effects on the K^+ channel currents and withdrawal thresholds. Pearson's correlation was used to determine the distance of clustered genes, and similarities among samples. Principal Component Analysis was calculated by princomp function in R based on correlation matrix, and PCA ellipse calculation, used to compare the clusters distance, was based on Square Mahalanobis distance metric [64]. Canonical Pathway enrichment calculated with Ingenuity Pathways Analysis is based on the right-tailed Fisher exact test. A P value of less than 0.05 was considered statistically significant.

Supplementary Material

Refer to Web version on PubMed Central for supplementary material.

Acknowledgments

We wish to thank Dr. Caretha L. Creasy from GlaxoSmithKline Laboratories for generously providing GSK503 and Dr. Walter N. Hittleman at MD Anderson Cancer Center for assisting with the confocal microscopy. We also thank Dr. Zhizhong Pan at MD Anderson Cancer Center and Dr. Fan Wang at Duke University for providing the $G9a^{flox/flox}$ and $Advillin^{Cre}$ mice, respectively. This study was supported by the NIH Blueprint for Neuroscience Research – Grand Challenge on Chronic Pain (grant # R01 DE022015) and by the N.G. and Helen T. Hawkins endowment (to H.-L.P.).

List of IUPHAR nomenclature of K+ channels and their gene symbols used

K_v1.2	Kcna2
K_v1.4	Kcna4
K_v4.2	Kcnd2
K_v4.3	Kcnd3
K_v7.2	Kcnq2
K_v9.1	Kcns1
BKα1	Kcnma1

List of abbreviations

BK	large-conductance Ca^{2+}-activated K^+ channel
ChIP	chromatin immunoprecipitation

DRG	dorsal root ganglion
EZH2	enhancer of zeste homolog-2
G9a	euchromatic histone-lysine N-methyltransferase 2 (*Ehmt2*)
GLP	G9a-like protein
HDAC	histone deacetylase
Kv	voltage-gated K^+ channel
SAHA	suberoxylanilide hydroxamic acid
SNL	spinal nerve ligation
TSS	transcriptional start site

References

Internet website: http://genome.ucsc.edu/cgi-bin/hgGateway

1. Amir R, Michaelis M, Devor M. Burst discharge in primary sensory neurons: triggered by subthreshold oscillations, maintained by depolarizing afterpotentials. J Neurosci. 2002; 22:1187–1198. [PubMed: 11826148]
2. Campbell JN, Raja SN, Meyer RA, Mackinnon SE. Myelinated afferents signal the hyperalgesia associated with nerve injury. Pain. 1988; 32:89–94. [PubMed: 3340426]
3. Wang H, et al. Chronic neuropathic pain is accompanied by global changes in gene expression and shares pathobiology with neurodegenerative diseases. Neuroscience. 2002; 114:529–546. [PubMed: 12220557]
4. Xiao HS, et al. Identification of gene expression profile of dorsal root ganglion in the rat peripheral axotomy model of neuropathic pain. Proc Natl Acad Sci U S A. 2002; 99:8360–8365. [PubMed: 12060780]
5. Cao XH, Byun HS, Chen SR, Cai YQ, Pan HL. Reduction in voltage-gated K+ channel activity in primary sensory neurons in painful diabetic neuropathy: role of brain-derived neurotrophic factor. J Neurochem. 2010; 114:1460–1475. [PubMed: 20557422]
6. Chen SR, Cai YQ, Pan HL. Plasticity and emerging role of BKCa channels in nociceptive control in neuropathic pain. J Neurochem. 2009; 110:352–362. [PubMed: 19457113]
7. Rasband MN, et al. Distinct potassium channels on pain-sensing neurons. Proc Natl Acad Sci U S A. 2001; 98:13373–13378. [PubMed: 11698689]
8. Rose K, et al. Transcriptional repression of the M channel subunit Kv7.2 in chronic nerve injury. Pain. 2011; 152:742–754. [PubMed: 21345591]
9. Mucha M, et al. Transcriptional control of KCNQ channel genes and the regulation of neuronal excitability. J Neurosci. 2010; 30:13235–13245. [PubMed: 20926649]
10. Vydyanathan A, Wu ZZ, Chen SR, Pan HL. A-type voltage-gated K+ currents influence firing properties of isolectin B4-positive but not isolectin B4-negative primary sensory neurons. J Neurophysiol. 2005; 93:3401–3409. [PubMed: 15647393]
11. Cao XH, Chen SR, Li L, Pan HL. Nerve injury increases brain-derived neurotrophic factor levels to suppress BK channel activity in primary sensory neurons. J Neurochem. 2012; 121:944–953. [PubMed: 22428625]
12. Chien LY, Cheng JK, Chu D, Cheng CF, Tsaur ML. Reduced expression of A-type potassium channels in primary sensory neurons induces mechanical hypersensitivity. J Neurosci. 2007; 27:9855–9865. [PubMed: 17855600]

13. Delmas P, Brown DA. Pathways modulating neural KCNQ/M (Kv7) potassium channels. Nat Rev Neurosci. 2005; 6:850–862. [PubMed: 16261179]
14. Marrion NV, Tavalin SJ. Selective activation of Ca2+-activated K+ channels by co-localized Ca2+ channels in hippocampal neurons. Nature. 1998; 395:900–905. [PubMed: 9804423]
15. Sah P, Faber ES. Channels underlying neuronal calcium-activated potassium currents. Prog Neurobiol. 2002; 66:345–353. [PubMed: 12015199]
16. Riccio A. Dynamic epigenetic regulation in neurons: enzymes, stimuli and signaling pathways. Nat Neurosci. 2010; 13:1330–1337. [PubMed: 20975757]
17. Guan JS, et al. HDAC2 negatively regulates memory formation and synaptic plasticity. Nature. 2009; 459:55–60. [PubMed: 19424149]
18. Kouzarides T. Chromatin modifications and their function. Cell. 2007; 128:693–705. [PubMed: 17320507]
19. Ronan JL, Wu W, Crabtree GR. From neural development to cognition: unexpected roles for chromatin. Nat Rev Genet. 2013; 14:347–359. [PubMed: 23568486]
20. Everill B, Kocsis JD. Reduction in potassium currents in identified cutaneous afferent dorsal root ganglion neurons after axotomy. J Neurophysiol. 1999; 82:700–708. [PubMed: 10444667]
21. Passmore GM, et al. KCNQ/M currents in sensory neurons: significance for pain therapy. J Neurosci. 2003; 23:7227–7236. [PubMed: 12904483]
22. Kim SH, Chung JM. An experimental model for peripheral neuropathy produced by segmental spinal nerve ligation in the rat. Pain. 1992; 50:355–363. [PubMed: 1333581]
23. Broide RS, et al. Distribution of histone deacetylases 1-11 in the rat brain. J Mol Neurosci. 2007; 31:47–58. [PubMed: 17416969]
24. Rivera C, et al. The K+/Cl− co-transporter KCC2 renders GABA hyperpolarizing during neuronal maturation. Nature. 1999; 397:251–255. [PubMed: 9930699]
25. Vedadi M, et al. A chemical probe selectively inhibits G9a and GLP methyltransferase activity in cells. Nat Chem Biol. 2011; 7:566–574. [PubMed: 21743462]
26. Beguelin W, et al. EZH2 is required for germinal center formation and somatic EZH2 mutations promote lymphoid transformation. Cancer Cell. 2013; 23:677–692. [PubMed: 23680150]
27. Dokmanovic M, Clarke C, Marks PA. Histone deacetylase inhibitors: overview and perspectives. Mol Cancer Res. 2007; 5:981–989. [PubMed: 17951399]
28. Cai YQ, et al. Role of M2, M3, and M4 muscarinic receptor subtypes in the spinal cholinergic control of nociception revealed using siRNA in rats. J Neurochem. 2009; 111:1000–1010. [PubMed: 19780895]
29. Luo MC, et al. An efficient intrathecal delivery of small interfering RNA to the spinal cord and peripheral neurons. Mol Pain. 2005; 1:29. [PubMed: 16191203]
30. Gupta-Agarwal S, et al. G9a/GLP histone lysine dimethyltransferase complex activity in the hippocampus and the entorhinal cortex is required for gene activation and silencing during memory consolidation. J Neurosci. 2012; 32:5440–5453. [PubMed: 22514307]
31. Zhou X, et al. Deletion of PIK3C3/Vps34 in sensory neurons causes rapid neurodegeneration by disrupting the endosomal but not the autophagic pathway. Proc Natl Acad Sci U S A. 2010; 107:9424–9429. [PubMed: 20439739]
32. Mortazavi A, Williams BA, McCue K, Schaeffer L, Wold B. Mapping and quantifying mammalian transcriptomes by RNA-Seq. Nat Methods. 2008; 5:621–628. [PubMed: 18516045]
33. Kim DS, Choi JO, Rim HD, Cho HJ. Downregulation of voltage-gated potassium channel alpha gene expression in dorsal root ganglia following chronic constriction injury of the rat sciatic nerve. Brain Res Mol Brain Res. 2002; 105:146–152. [PubMed: 12399117]
34. Zhao X, et al. A long noncoding RNA contributes to neuropathic pain by silencing Kcna2 in primary afferent neurons. Nat Neurosci. 2013; 16:1024–1031. [PubMed: 23792947]
35. Tsantoulas C, et al. Sensory neuron downregulation of the Kv9.1 potassium channel subunit mediates neuropathic pain following nerve injury. J Neurosci. 2012; 32:17502–17513. [PubMed: 23197740]

36. Fan L, et al. Impaired neuropathic pain and preserved acute pain in rats overexpressing voltage-gated potassium channel subunit Kv1.2 in primary afferent neurons. Mol Pain. 2014; 10:8. [PubMed: 24472174]
37. Ma C, Rosenzweig J, Zhang P, Johns DC, LaMotte RH. Expression of inwardly rectifying potassium channels by an inducible adenoviral vector reduced the neuronal hyperexcitability and hyperalgesia produced by chronic compression of the spinal ganglion. Mol Pain. 2010; 6:65. [PubMed: 20923570]
38. Uchida H, Sasaki K, Ma L, Ueda H. Neuron-restrictive silencer factor causes epigenetic silencing of Kv4.3 gene after peripheral nerve injury. Neuroscience. 2010; 166:1–4. [PubMed: 20006971]
39. Rice JC, et al. Histone methyltransferases direct different degrees of methylation to define distinct chromatin domains. Mol Cell. 2003; 12:1591–1598. [PubMed: 14690610]
40. Tachibana M, et al. G9a histone methyltransferase plays a dominant role in euchromatic histone H3 lysine 9 methylation and is essential for early embryogenesis. Genes Dev. 2002; 16:1779–1791. [PubMed: 12130538]
41. Tachibana M, et al. Histone methyltransferases G9a and GLP form heteromeric complexes and are both crucial for methylation of euchromatin at H3-K9. Genes Dev. 2005; 19:815–826. [PubMed: 15774718]
42. Chiechio S, et al. Epigenetic modulation of mGlu2 receptors by histone deacetylase inhibitors in the treatment of inflammatory pain. Mol Pharmacol. 2009; 75:1014–1020. [PubMed: 19255242]
43. Denk F, et al. HDAC inhibitors attenuate the development of hypersensitivity in models of neuropathic pain. Pain. 2013; 154:1668–1679. [PubMed: 23693161]
44. Zhang Y, Laumet G, Chen SR, Hittelman WN, Pan HL. Pannexin-1 up-regulation in the dorsal root ganglion contributes to neuropathic pain development. J Biol Chem. 2015; 290:14647–14655. [PubMed: 25925949]
45. Ghare SS, et al. Coordinated histone H3 methylation and acetylation regulate physiologic and pathologic fas ligand gene expression in human CD4+ T cells. J Immunol. 2014; 193:412–421. [PubMed: 24899502]
46. Park JA, et al. Deacetylation and methylation at histone H3 lysine 9 (H3K9) coordinate chromosome condensation during cell cycle progression. Mol Cells. 2011; 31:343–349. [PubMed: 21359677]
47. Chaturvedi CP, et al. Maintenance of gene silencing by the coordinate action of the H3K9 methyltransferase G9a/KMT1C and the H3K4 demethylase Jarid1a/KDM5A. Proc Natl Acad Sci U S A. 2012; 109:18845–18850. [PubMed: 23112189]
48. Lee DY, Northrop JP, Kuo MH, Stallcup MR. Histone H3 lysine 9 methyltransferase G9a is a transcriptional coactivator for nuclear receptors. J Biol Chem. 2006; 281:8476–8485. [PubMed: 16461774]
49. Vakoc CR, Mandat SA, Olenchock BA, Blobel GA. Histone H3 lysine 9 methylation and HP1gamma are associated with transcription elongation through mammalian chromatin. Mol Cell. 2005; 19:381–391. [PubMed: 16061184]
50. Laedermann CJ, Pertin M, Suter MR, Decosterd I. Voltage-gated sodium channel expression in mouse DRG after SNI leads to re-evaluation of projections of injured fibers. Mol Pain. 2014; 10:19. [PubMed: 24618114]
51. Chaplan SR, Bach FW, Pogrel JW, Chung JM, Yaksh TL. Quantitative assessment of tactile allodynia in the rat paw. J Neurosci Methods. 1994; 53:55–63. [PubMed: 7990513]
52. Renn CL, et al. Multimodal assessment of painful peripheral neuropathy induced by chronic oxaliplatin-based chemotherapy in mice. Mol Pain. 2011; 7:29. [PubMed: 21521528]
53. Bangaru ML, Park F, Hudmon A, McCallum JB, Hogan QH. Quantification of gene expression after painful nerve injury: validation of optimal reference genes. J Mol Neurosci. 2012; 46:497–504. [PubMed: 21863315]
54. Chen SR, Pan HL. Antinociceptive effect of morphine, but not mu opioid receptor number, is attenuated in the spinal cord of diabetic rats. Anesthesiology. 2003; 99:1409–1414. [PubMed: 14639157]
55. Subbanna S, et al. G9a-mediated histone methylation regulates ethanol-induced neurodegeneration in the neonatal mouse brain. Neurobiol Dis. 2013; 54:475–485. [PubMed: 23396011]

56. Wilting RH, et al. Overlapping functions of Hdac1 and Hdac2 in cell cycle regulation and haematopoiesis. EMBO J. 2010; 29:2586–2597. [PubMed: 20571512]
57. Zhang Z, Cai YQ, Zou F, Bie B, Pan ZZ. Epigenetic suppression of GAD65 expression mediates persistent pain. Nat Med. 2011; 17:1448–1455. [PubMed: 21983856]
58. Mandal M, et al. Epigenetic repression of the Igk locus by STAT5-mediated recruitment of the histone methyltransferase Ezh2. Nat Immunol. 2011; 12:1212–1220. [PubMed: 22037603]
59. Jelinek J, et al. Conserved DNA methylation patterns in healthy blood cells and extensive changes in leukemia measured by a new quantitative technique. Epigenetics. 2012; 7:1368–1378. [PubMed: 23075513]
60. Mitchell NC, et al. Hfp inhibits Drosophila myc transcription and cell growth in a TFIIH/Hay-dependent manner. Development. 2010; 137:2875–2884. [PubMed: 20667914]
61. Trapnell C, Pachter L, Salzberg SL. TopHat: discovering splice junctions with RNA-Seq. Bioinformatics. 2009; 25:1105–1111. [PubMed: 19289445]
62. Trapnell C, et al. Transcript assembly and quantification by RNA-Seq reveals unannotated transcripts and isoform switching during cell differentiation. Nat Biotechnol. 2010; 28:511–515. [PubMed: 20436464]
63. Malin SA, Davis BM, Molliver DC. Production of dissociated sensory neuron cultures and considerations for their use in studying neuronal function and plasticity. Nat Protoc. 2007; 2:152–160. [PubMed: 17401349]
64. Worley B, Halouska S, Powers R. Utilities for quantifying separation in PCA/PLS-DA scores plots. Anal Biochem. 2013; 433:102–104. [PubMed: 23079505]

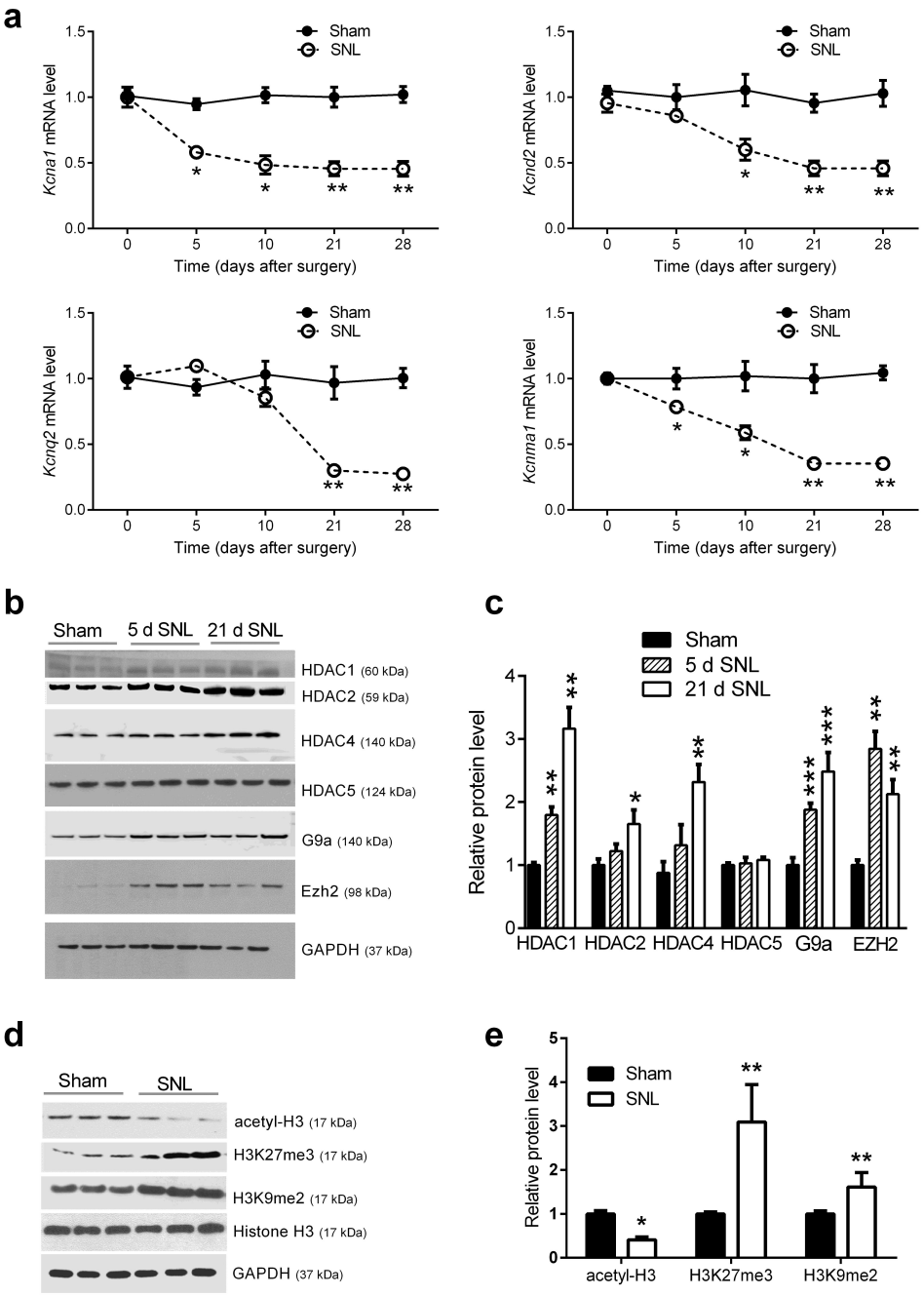

Figure 1. Nerve injury reduces expression levels of *Kcna4, Kcnd2, Kcnq2* and *Kcnma1* and increases expression and activity of HDACs, G9a and EZH2 in the DRG

(**a**) Time course of reduction in the mRNA level of *Kcna4, Kcnd2, Kcnq2* and *Kcnma1* in the DRG. The L5 and L6 DRGs were obtained from sham control and SNL rats before and at 5, 10, 21 and 28 days after surgery (n = 6 rats in each group). The mRNA of K^+ channels was quantified using real-time PCR and normalized to a housekeeping gene (*Gapdh*). **(b,c)** Western blot gel images and mean data show protein levels of HDAC1, HDAC2, HDAC4, HDAC5, G9a and EZH2 in L5 and L6 DRG tissues obtained from sham control and SNL rats at 5 and 21 days after surgery (n = 9 in each group). **(d,e)** Original gel images and

quantification data of the protein levels of acetyl-H3, H3K9me2, and H3K27me3 in the DRGs obtained from sham and SNL rats 21 days after surgery (n = 6 in each group). GAPDH was used as a loading control. Data are shown as mean ± s.e.m. Statistical analysis was performed using repeated-measures ANOVA or the Mann-Whitney test. * $P < 0.05$, ** $P < 0.01$, *** $P < 0.001$, compared with the respective baseline value. Supplementary Figure S8 contains the uncropped version of the gel images.

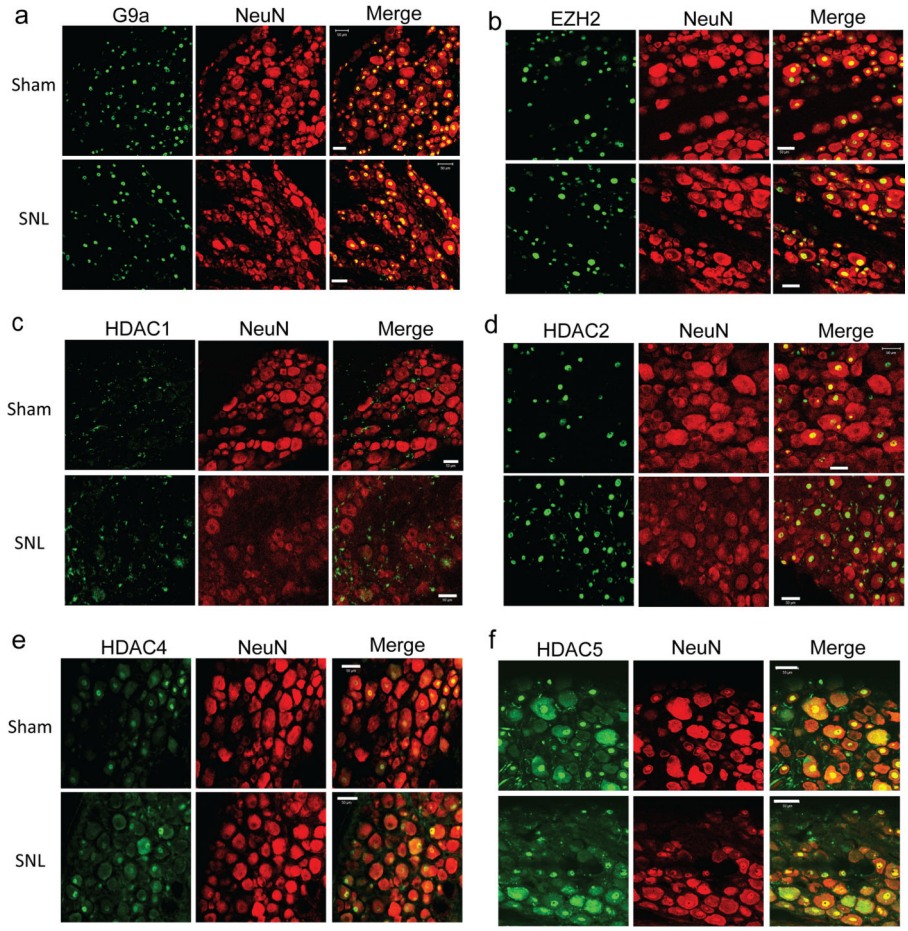

Figure 2. Cellular distribution of HDACs, G9a and EZH2 in control and injured DRGs

(a-f) Double immunostaining and confocal images show co-localization of G9a (**a**), EZH2 (**b**), HDAC2 (**d**), HDAC4 (**e**) and HDAC5 (**f**), but not HDAC1 (**c**), with a neuronal marker (NeuN, red) in DRG sections from sham and SNL rats 21 days after surgery. N = 4 rats in each condition. Scale bar, 50 μm. In each panel, digitally merged images are shown at right.

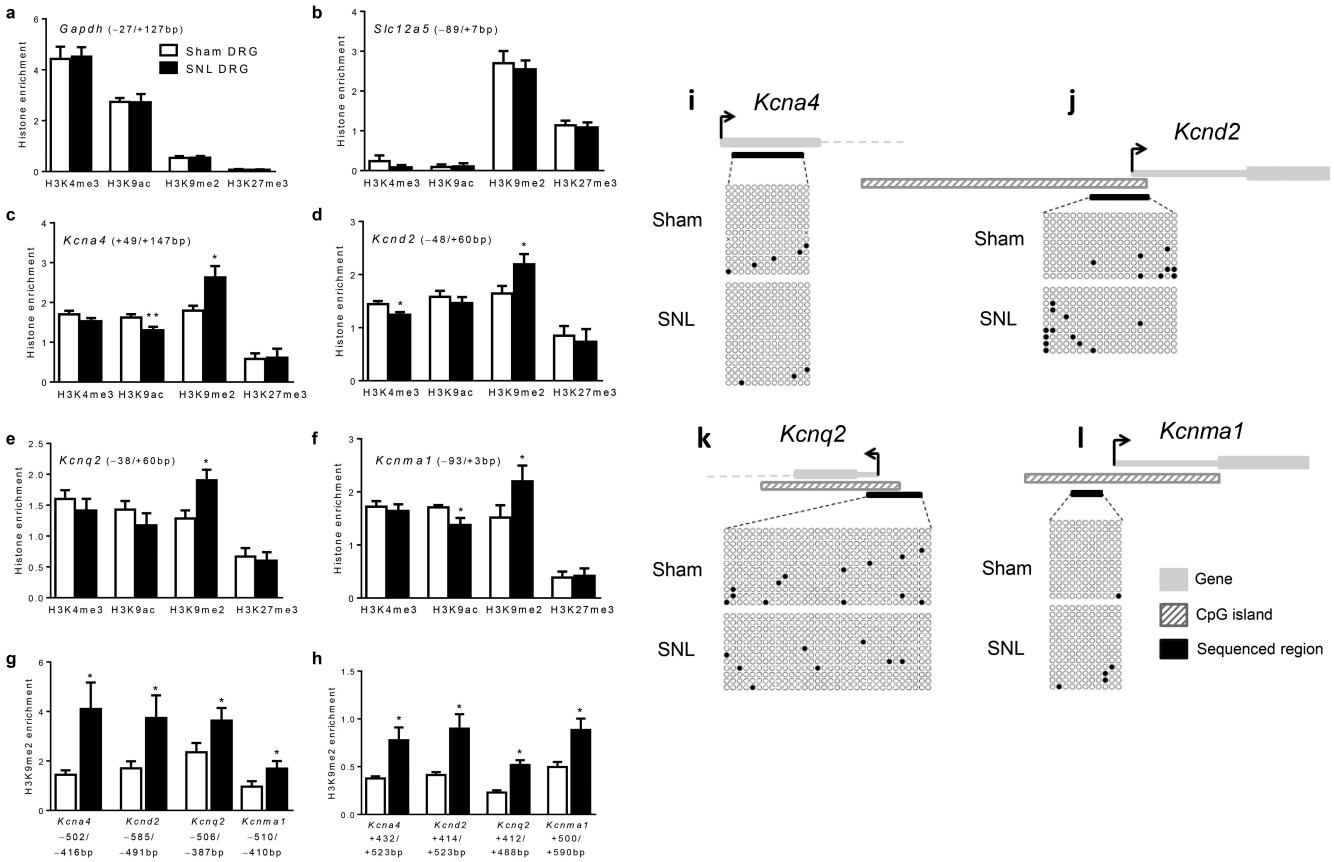

Figure 3. Nerve injury increases H3K9me2 levels at K^+ channel promoters but does not change DNA methylation status at their promoter regions in the DRG

(**a-f**) ChIP-PCR quantification data show the levels of two activating histone marks (H3K4me3 and H3K9ac) and two repressive histone marks (H3K9me2 and H3K27me3) around the TSS of *Gapdh* (**a**), *Slc12a5* (**b**), *Kcna4* (**c**), *Kcnd2* (**d**), *Kcnq2* (**e**) and *Kcnma1* (**f**) in the DRG obtained from sham control and SNL rats 3 weeks after surgery (n = 7 independent experiments in each group). (**g,h**), ChIP-PCR quantification data show the enrichment levels of H3K9me2 at the two different promoter regions of *Kcna4*, *Kcnd2*, *Kcnq2* and *Kcnma1* in the DRG obtained from sham control and SNL rats 3 weeks after surgery (n = 7 independent experiments in each group). PCR-targeted promoter regions are indicated in the parenthesis in each panel. Data were normalized by input and total H3 values and are presented as mean ± SEM. * $P < 0.05$, ** $P < 0.01$, compared with sham control group (Mann-Whitney test). (**i-l**) Bisulfite sequencing PCR analysis of *Kcna4* (**i**), *Kcnd2* (**j**), *Kcnq2* (**k**) and *Kcnma1* (**l**) in L5 and L6 DRGs obtained from sham control and SNL rats 21 days after surgery (n = 3 independent experiments in each group). The DNA methylation pattern of CpG sites near the TSS was analyzed. Each row represents the methylation pattern of a single clone. Open circles represent unmethylated CpG sites, and closed circles represent methylated CpG sites at the TSS.

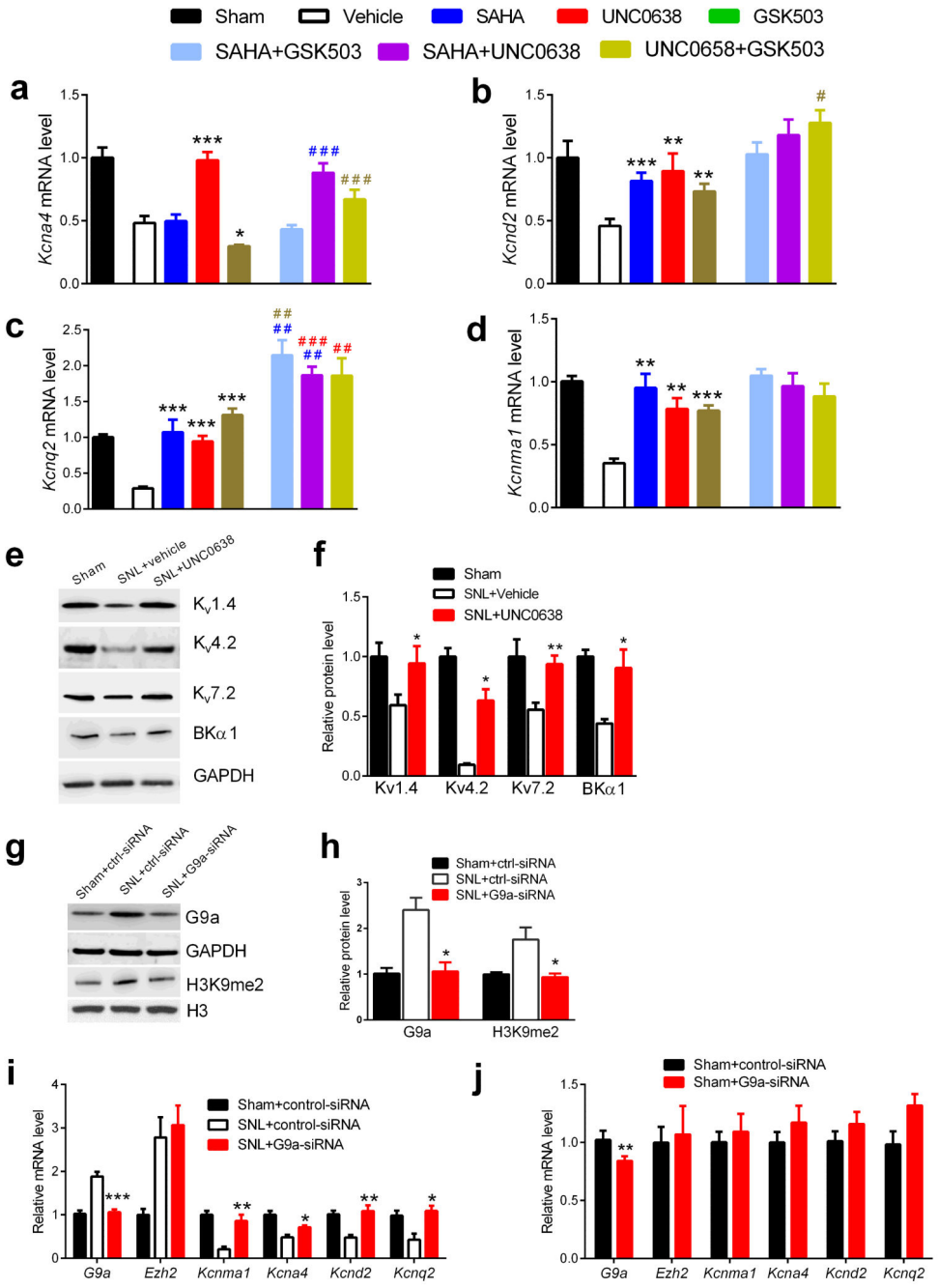

Figure 4. Inhibition of G9a activity normalizes K^+ channel gene expression in the DRG diminished by nerve injury

(**a-d)** Effects of intrathecal treatments with vehicle (n = 10), SAHA (50 μg, n = 9), UNC0638 (10 μg, n = 8), GSK503 (5 μg, n = 10), SAHA plus GSK503 (n = 8), SAHA plus UNC0638 (n = 9) or UNC0638 plus GSK503 (n = 8) on the mRNA levels of *Kcna4* (**a**), *Kcnd2* (**b**), *Kcnq2* (**c**), and *Kcnma1* (**d**) in the DRG obtained from SNL rats 28 days after surgery. Data from sham control rats were plotted as the control (n = 6 rats). (**e,f**) Effects of nerve injury and UNC0638 on the protein levels of Kv1.4, Kv4.2, Kv7.2 and BKα1 in the

L5 and L6 DRG (n = 6 rats in each group). (**g,h**) Effect of G9a-specific siRNA on the G9a and H3K9me2 protein levels in the DRG obtained from SNL rats 24 h after the last injection (n = 5 in each group). (**i,j**) Effects of G9a-specific siRNA on the mRNA levels of *G9a, Ezh2, Kcna4, Kcnd2, Kcnq2* and *Kcnma1* in the DRG obtained from SNL (**i**) and sham control (**j**) rats 24 h after the last injection (n = 10 in each group). Data are presented as mean ± s.e.m. Statistical analysis was performed using two-way ANOVA followed by Bonferroni's *post hoc* tests (**a-d**), one-way ANOVA (**f,h,i**), or Mann-Whitney test (**j**). * $P < 0.05$, ** $P < 0.01$, *** $P < 0.001$, compared with the vehicle-treated group (**a-f**) or SNL + control-siRNA group (**g-j**). # $P < 0.05$, ## $P < 0.01$, ### $P < 0.001$, compared with the same color used for treatment with the single inhibitor (**a-d**). Supplementary Figure S9 contains the uncropped version of the gel images.

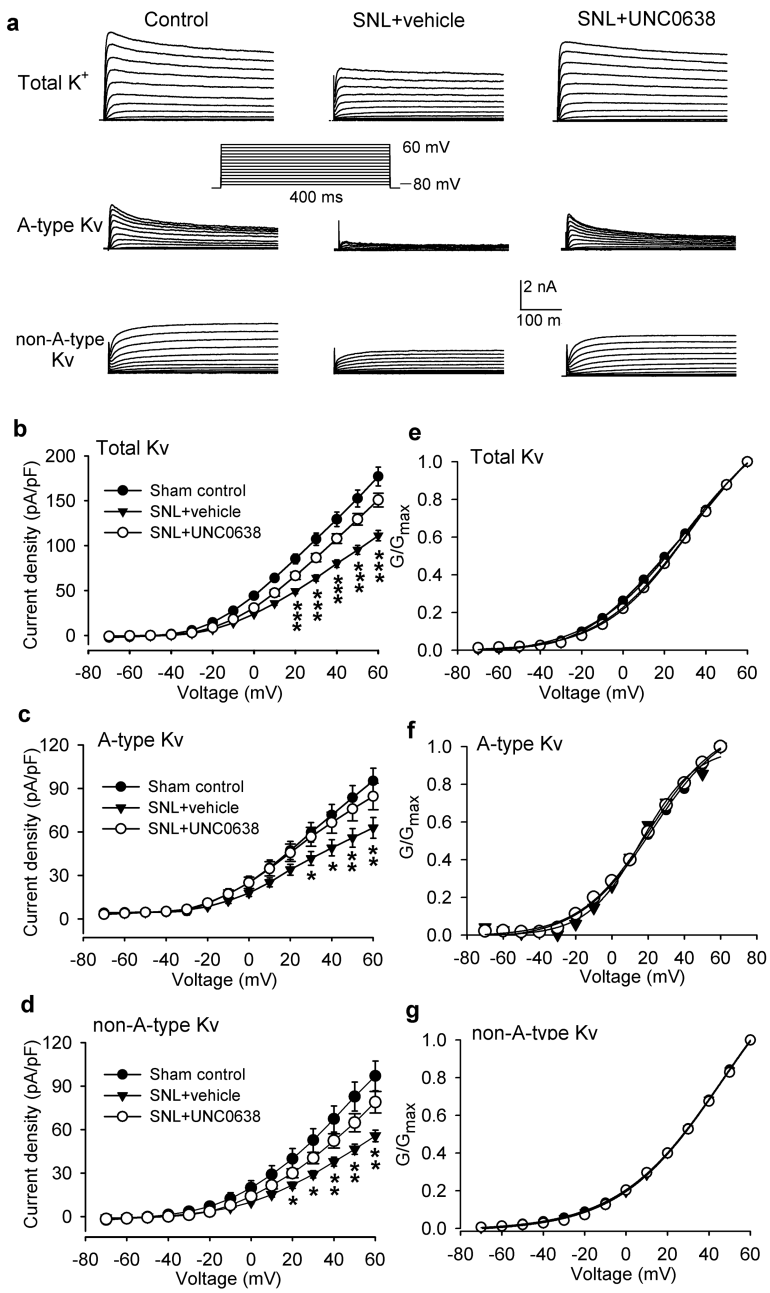

Figure 5. Inhibition of G9a activity restores Kv channel currents in DRG neurons reduced by nerve injury

(**a**) Original traces of total whole-cell Kv currents, A-type Kv currents, and non-A-type Kv currents in DRG neurons from sham control rats, SNL rats treated with vehicle, and SNL rats treated with UNC0638. Neurons were held at −80 mV and depolarized from −70 to 60 mV in 10-mV increments (inset). (**b-d)** Current densities of total whole-cell Kv currents (**b,** n = 21 neurons in each group, n = 5 rats in each group), A-type Kv currents (**c,** n = 16 neurons in each group, n = 5 rats in each group), and non-A-type Kv currents (**d,** n = 16 neurons in each group, n = 5 rats in each group) in DRG neurons dissociated from control rats, SNL rats treated with vehicle and SNL rats treated with UNC0638. (**e-g**) The

conductance–voltage (G–V) curves of total and A-type Kv currents in DRG neurons from control and SNL rats treated with UNC0638 or vehicle. The $V_{0.5}$ values of total Kv currents (control, 31.1 ± 1.7 mV; SNL+vehicle, 33.0 ± 1.0 mV; SNL+UNC0638, 32.5 ± 1.2 mV), A-type Kv currents (control, 19.7 ± 3.2 mV; SNL+vehicle, 16.0 ± 5.3 mV; SNL+UNC0638, 16.8 ± 4.3 mV) and non-A-type Kv currents (control, 46.4 ± 1.3 mV; SNL+vehicle, 45.2 ± 1.0 mV; SNL+UNC0638, 45.9 ± 3.2 mV) were not significantly different between the three groups. There was no significant difference in the *k* value of total Kv currents (control, 24.6 ± 1.1 mV; SNL+vehicle, 22.3 ± 0.6 mV; SNL+UNC0638, 21.1 ± 0.8 mV), A-type Kv currents (control, 19.6 ± 1.9 mV; SNL+vehicle, 13.7 ± 1.3 mV; SNL+UNC0638, 15.1 ± 1.5 mV) and non-A-type Kv currents (control, 25.0 ± 0.5 mV; SNL+vehicle, 24.3 ± 0.4 mV; SNL+UNC0638, 24.7 ± 1.3 mV) between the three groups. Data are presented as mean ± s.e.m. * $P < 0.05$, ** $P < 0.01$, *** $P < 0.001$, compared with the corresponding value in the control group (two-way ANOVA).

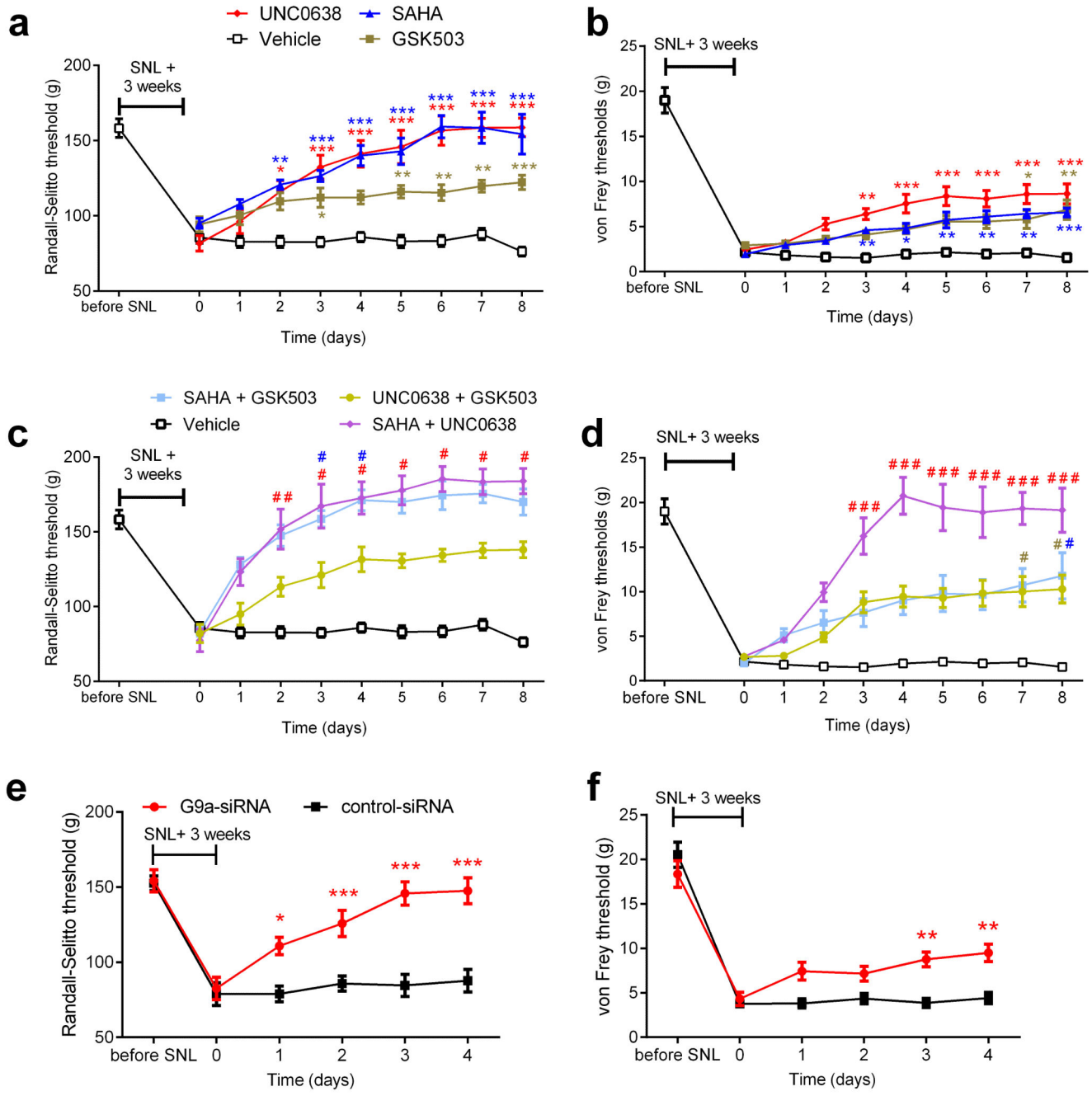

Figure 6. Differential effects of inhibition of G9a, HDACs and EZH2 on pain hypersensitivity induced by nerve injury

(**a,b**) Effects of intrathecal injections of vehicle (n = 12), UNC0638 (10 μg, n = 12), SAHA (50 μg, n = 12) or GSK503 (5 μg, n = 10) on the Randall-Selitto and von Frey withdrawal thresholds of SNL rats 3 weeks after surgery. (**c,d**) Effects of intrathecal treatments with UNC0638 plus SAHA (n = 9), UNC0638 plus GSK503 (n = 8) and SAHA plus GSK503 (n = 10) on the Randall-Selitto and von Frey thresholds of SNL rats. Drugs were injected intrathecally daily for 8 days starting 3 weeks after surgery, and each behavior test was performed 24 h after each treatment. (**e,f**) Effects of intrathecal treatment with control- and

G9a-specific siRNA on the Randall-Selitto and von Frey thresholds of SNL rats of SNL rats (n = 12 rats in each group). Data are presented as mean ± s.e.m. Statistical analysis was performed using two-way ANOVA followed by Bonferroni's *post hoc* tests. * P < 0.05, ** P < 0.01, *** P < 0.001, compared with the baseline control (**a,b,e,f**). # P < 0.05, ## P < 0.01, ### P < 0.001, compared with the same color used for treatment with the single inhibitor (**c,d**).

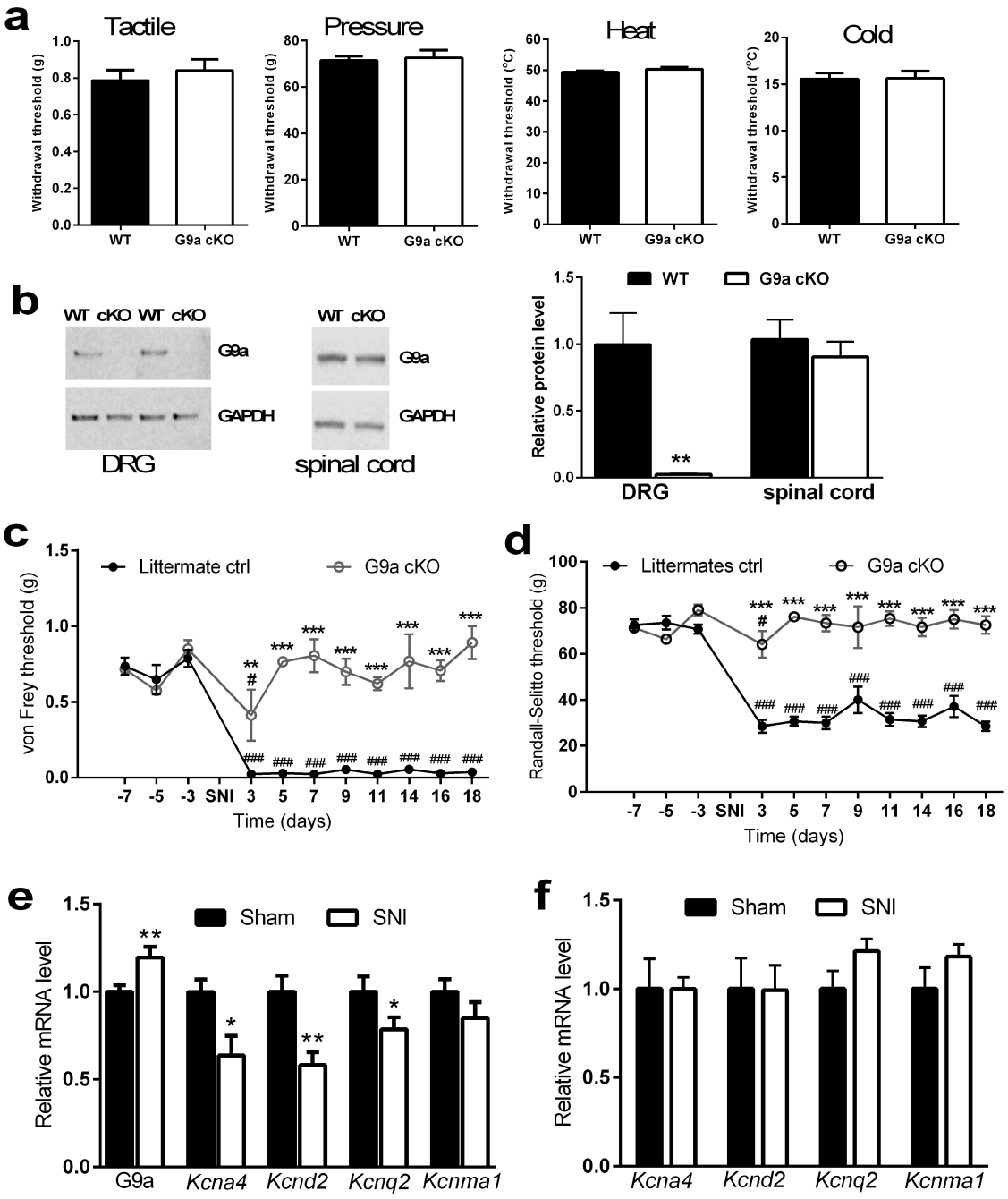

Figure 7. Genetic deletion of G9a in DRG neurons prevents nerve injury-induced pain hypersensitivity and reduction in K^+ channel gene expression in the DRG

(**a**) Comparison of the von Frey (n = 6), Randall-Selitto (n = 6), heat (n = 5), and cold (n = 5) withdrawal thresholds between G9a condition KO and wild-type control mice. (**b**) Original gel images and mean data show the effects of G9a conditional deletion on the protein level of G9a in the lumbar DRGs and the dorsal spinal cord (n = 5 mice in each group). (**c,d**) Time course of changes in the Randall-Selitto and von Frey withdrawal thresholds of G9a conditional KO (cKO, n = 6) and littermate control ($G9a^{flox/flox}$, n = 7) mice before and after speared nerve injury (SNI). (**e,f**) Quantitative PCR data show the

mRNA levels of G9a, *Kcna4, Kcnd2, Kcnq2* and *Kcnma1* in the DRG obtained from wild-type controls (sham, n = 11; SNI, n = 11; **e**) and G9a cKO (sham, n = 6; SNI, n = 6; **f**) mice 21 days after surgery. Data are presented as mean ± s.e.m. Statistical analysis was performed using Mann-Whitney U test (**a**), one-way ANOVA followed by Bonferroni's *post hoc* tests (**b**), two-way ANOVA followed by Bonferroni's *post hoc* tests (**c,d**) or Mann-Whitney test (**e,f**). * $P < 0.05$, ** $P < 0.01$, *** $P < 0.001$, compared with the littermate control at the same time point (**c,d**) or the respective sham control (**e,f**). # $P < 0.05$, ## $P < 0.01$, ### $P < 0.001$, compared with the respective baseline control (3 day). Supplementary Figure S10 contains the uncropped version of the gel images.

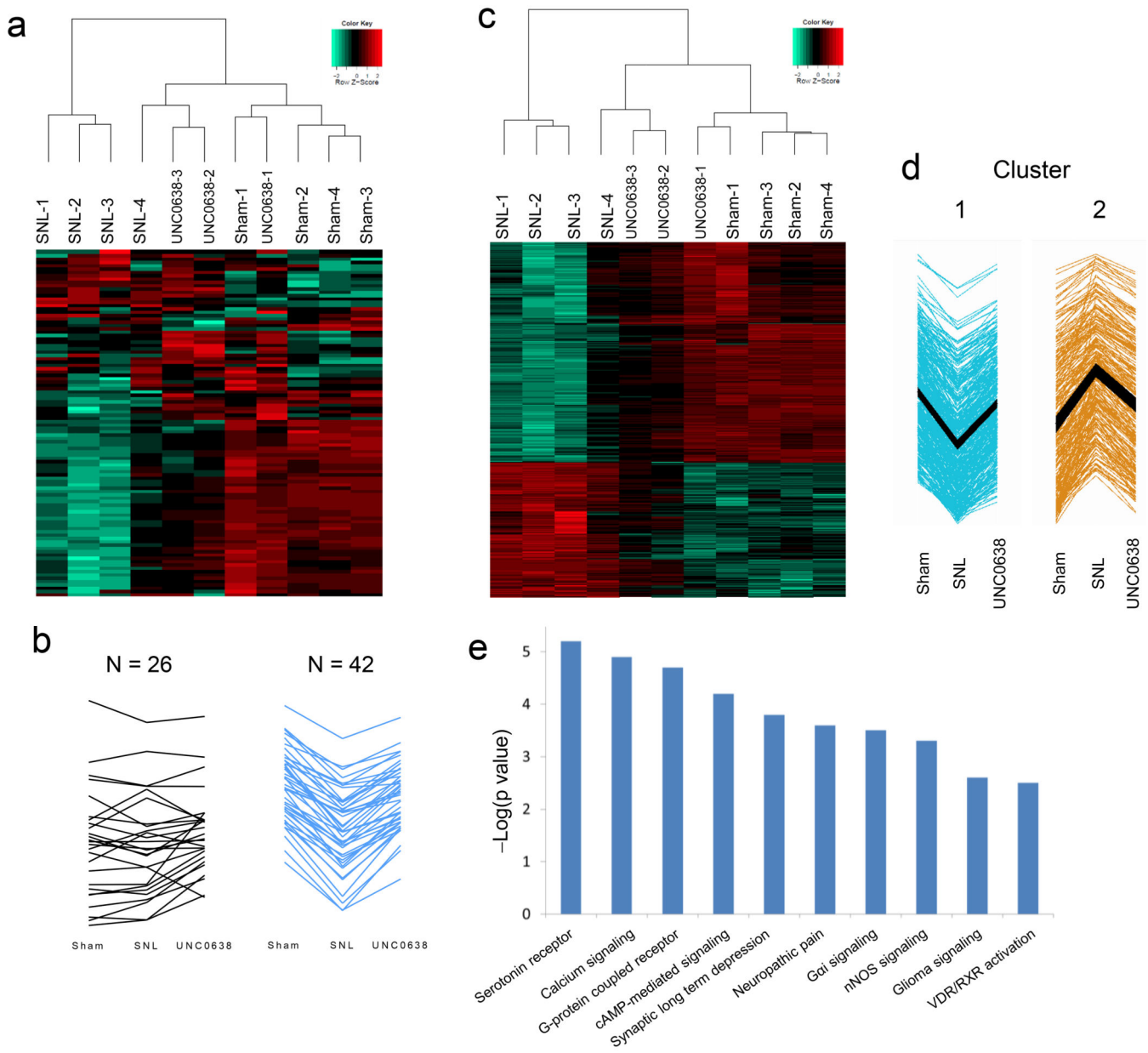

Figure 8. G9a inhibition normalizes the expression level of K^+ channel genes and a subset of other genes modified by nerve injury

(**a**) Heat map generated with the expression values of 105 K^+ channel-related genes found among the 16,876 mapped genes. The small dendrogram at top shows clustering of the samples regarding these expression values (4 rats in the sham group, 4 rats in the SNL group, and 3 SNL rats treated with UNC0638). (**b**) Scattered line plots (K-means clustering) show the effect of UNC0638 on individual K^+ channel gene expression in the DRG, grouped according to their responses to nerve injury: down-regulated (n = 42), up-regulated (n = 4, not plotted), and no change (n = 26). (**c**) Heat map representing the expression values for the 638 genes that were modified at least two fold by nerve injury and normalized to the control level after treatment with UNC0638. (**d**) The 638 genes were separated into two clusters (K-

means clustering) according to their changes in expression due to SNL and UNC0638 treatment. (**e**) Ingenuity Pathway Analysis showed the principal canonical pathways for the 638 genes shown in **c** and **d**.